Future changes in the mean and variability of extreme rainfall indices over the Guinea Coast and role of the Atlantic equatorial mode

Koffi Worou[1], Thierry Fichefet[1], and Hugues Goosse[1]

[1]Georges Lemaître Centre for Earth and Climate Research (TECLIM), Earth and Life Institute (ELI), Université catholique de Louvain (UCLouvain), Louvain-la-Neuve, Belgium

Correspondence: Koffi Worou (koffi.worou@uclouvain.be)

Abstract. The occurrence of climate extremes could have dramatic impacts on various sectors such as agriculture, water supply, and energy production. Over the last decades, less frequent and more intense rainfalls have been observed in the coastal areas of West Africa (the Guinea Coast). Part of this variability in the extreme rainfalls can be related to the Atlantic equatorial mode (AEM) whose positive phases are associated with an enhancement of the mean rainfall over the Guinea Coast and an increase

5   in the intensity and frequency of rainfall events. The climate models that participate in the sixth phase of the Coupled Model Intercomparison Project (CMIP6) simulate reasonably well the rainfall extremes over the Guinea Coast and West Africa. However, less attention has been paid to the evaluation of the modelled rainfall extremes associated with the AEM under different climate conditions, while the variability of the AEM is expected to decrease in the future. Here, we use historical and SSP5-8.5 simulations from 24 models that contributed to CMIP6 to investigate the near-term, mid-term and long-term

10   future links between the AEM and the extreme rainfall events over the Guinea Coast. The extreme rainfall responses to the AEM are reasonably well represented over the 1995-2014 period, although there are substantial biases in their magnitudes. Future changes indicate an increase in the mean and variability of the majority of the extreme indices over the Guinea Coast. The average across the 12 indices of their percentage of long-term changes in mean and variability equals to $+10.46\%$ and $+16.44\%$, respectively. By contrast, the decreased variability of the AEM in a warmer climate leads to a reduced magnitude

15   of the rainfall extreme responses associated to AEM over the Guinea Coast. The multi-model median values of the long-term changes in the variance explained by the AEM for the different extreme indices range between -8.25% and -64.97%. As a consequence, while in absolute there is a projected increase in the variability of most of the extreme rainfall indices, the contribution of the AEM to this variability weakens in a warmer future climate.

1   Introduction

20   Extreme rainfall events are climatic hazards that could have damaging impacts on the life of people living in the affected regions. For example, during July and August 2012, more than 1.5 million West and Central African people experienced severe flash flood events (United Nations Office for the Coordination of Humanitarian Affairs (OCHA), 2012, 2021). Fofana et al. (2022) reported that over the period 1982-2019, one-third of the flooding events in Bamako were caused by severely abnormal

rainfalls. In 2019, the flooding of the Niger River after heavy rainfall affected 211 366 people, destroyed 16 375 houses, and killed 57 people (Elagib et al., 2021). In the northern part of Togo, more than 57 000 people were affected by intense rainfalls that occurred in October 2020, with the Oti River bursting its banks and flooding the surrounding areas, leading to 11 dead and 4000 buildings damaged (https://floodlist.com/africa/togo-oti-river-floods-october-2020, last access: 20-04-2021). For people born in 2021 in the Sub-Saharan Africa, the exposure to river flooding events is expected to increase 4.6, 8, and 8.6 times more than without climate change, in a world where global warming is limited to $1.5\,°C$, or where global warming reaches $2.4\,°C$ or $3.5\,°C$ by 2100, respectively (https://myclimatefuture.info/, last access: 11-08-2022). This increase is two to fourfold higher than the flooding events experienced by people in the same area, born in 1960, and highlights the climate urgency in reducing our greenhouse gas emissions for the safety of young people (Thiery et al., 2021).

The Sixth Assessement Report (AR6) of the Intergovernmental Panel on Climate Change (IPCC) stated that there is a low confidence in the observed heavy precipitation trend over West Africa for the last decades, as well as in the contribution of human influence to that trend (Seneviratne et al., 2021). However, there are some regional differences in the observed trends. For instance, in Nigeria, Dike et al. (2020) reported a significant increasing trend of the total wet-day rainfall amount, the maximum consecutive 5 days rainfall and the rainfall intensity in the June-September season over the period 1975-2013. Furthermore, they stated that the occurrence of flooding events in Nigeria could be attributed to the intensification of rainfall extremes.

Over the period 1961-2000, the observations indicate a decrease in the annual rainfall in southern Nigeria, with, however, an increase in the intensity of the daily rainfall and the annual maximum 1 day rainfall (New et al., 2006). Moreover, Bichet and Diedhiou (2018) demonstrated that over the 1981-2014 period, one the one hand, there is no overall clear significant trend in the mean April-June (AMJ) rainfall over Guinea Coast. However, north (south) of $7\,°N$ they observed a negative (positive) trend in the rainfall intensity and the rainfall intensity during wet spells, and an overall positive trend in the rainfall intensity during isolated wet days, with a tendency to a decrease in the rainfall occurrence. On the other, for the mean rainfall, rainfall intensity, rainfall intensity during isolated wet days and rainfall intensity during wet spells, a dominant positive trend is obtained over Guinea Coast during the September-November season, with a tendency to an increasing frequency of the rainfall events.

In addition, Odoulami and Akinsanola (2017) showed a significant negative trend in the June-September mean daily rainfall over the Guinea Coast during the 1998-2013 period, which represents up to 4% of the seasonal daily mean rainfall. Nevertheless, they found a decrease in the frequency of rainfall events higher than the 95th percentile, as well as a decrease in the contribution of these extreme events to the total annual rainfall. They also observed an overall upward and insignificant trend in the number of dry days over that area and a significant decreasing trend in the number of wet days.

More specifically, on an annual basis, Kpanou et al. (2020) showed that, during 1981-2015, coastal areas in the southwestern Côte d'Ivoire, Togo, and Bénin experienced an increasing trend in the total annual rainfall, which is associated with an increasing trend in the number of days with rainfall exceeding the 95th percentile and their contribution to the total rainfall. However, they found no clear trend in the total rainfall over the southern Ghana, where a significant increasing trend in both the number of days with rainfall exceeding the 95th percentile and their contribution to the total annual rainfall compensate with both a significant decreasing trend in the number of days with rainfall below the 95th percentile and their contribution to

the total annual rainfall.

60

The climate General Circulation Models (GCMs) participating in the sixth phase of the Coupled Models Intercomparison Project (CMIP6) simulate reasonably well the spatial distribution of the rainfall extreme indices in West Africa, with however different levels of intensity (Faye and Akinsanola, 2021; Klutse et al., 2021). Particularly, these models overestimate the frequency of wet days and the largest number of consecutive wet days (CWD, Table 2), and present positive biases in the heavy

65 and very heavy rainfalls (R10mm and R20mm, respectively) over areas with a complex topography. Furthermore, the modelled mean maximum wet spell lengths are not in accordance with observations (Klutse et al., 2021). The climate models show, however, a good spatial pattern of the mean maximum dry spell length. Regional Climate Models (RCMs) forced with CMIP5 GCMs outputs also show a good performance in simulating the spatial distribution of the present-day mean rainfall, maximum number of consecutive dry days and the total rainfall exceeding 95th percentile over West Africa (Akinsanola et al., 2020).

70

Extreme rainfall events are projected to intensify in a climate with a high anthropogenic emission of greenhouse gases (Rind et al., 1989; Mearns et al., 1995; Hegerl et al., 2015; Diedhiou et al., 2018; Akinsanola et al., 2020; van der Wiel and Bintanja, 2021; Li et al., 2021a; Dosio et al., 2021). Under the shared socioeconomic pathway scenarios, Li et al. (2021a) showed a long-term increase in the frequency and intensity of the maximum 1 day (RX1day) and 5 days (RX5day) rainfall in nearly

75 all the regions of the globe. At a regional scale, van der Wiel and Bintanja (2021) found that, over West Africa, the heavy rainfall events exceeding the 98th rainfall percentile will increase in a warmer climate. Under the Representative Concentration Pathway (RCP) 4.5 forcing scenario, projections carried out within RCM-CMIP5 suggest a future decrease of the total wet-day precipitation (PRCPTOT) in the Savannah-Sahel region, and an increase in the western Guinea Coast (westward of $0\,°E$) (Akinsanola and Zhou, 2019). This pattern is more amplified under the RCP8.5 forcing scenario.

80 These simulations also show an overall increase in the number of days with rainfall exceeding $10\,mm$ (R10mm) and $20\,mm$ (R20mm) in the Guinea Coast and the Savannah regions. The amount of rainfall during very wet days (R95pTOT), the RX5day and the simple daily rainfall intensity (SDII) also increase over the Guinea Coast, the Savannah and the Sahel areas. This means an increasing intensity of rainfall and wet extreme rainfall, which would exacerbate the risk of more frequent floods in the West Africa. Akinsanola and Zhou (2019) reported an overall future decrease in CWD over the West Africa, except along

85 the coastline in the West. With respect to the change in the maximum consecutive dry days (CDD), there is a decrease (an increase) in the western (eastern) areas of the Guinea Coast.

Analyses of RCP4.5 and RCP8.5 projections with RCMs demonstrated an increase in the West African rainfall variability, which is associated with enhanced mean rainfall and rainfall extremes in the Guinea Coast (Akinsanola et al., 2020). There is an

90 increased variability of the June-September (JJAS) daily rainfall under RCP4.5 and RCP8.5 (larger magnitude) forcing scenarios, relative to the present-day conditions (10-28%). The increase of the rainfall variability in the Guinea Coast is present from the synoptic to intraseasonal timescales, with a large spread of the models on the annual timescale. This increased variability is dominated by an increased coefficient of variation of the rainfall (the ratio between the standard deviation of the rainfall and

the rainfall climatology), alongside with an increased mean rainfall in the western areas of the Guinea Coast. Overall, a large
95 part of this increased rainfall variability in West Africa can be explained by the change in the water vapour in a warmer world
following the Clausius Clapeyron equation (Akinsanola et al., 2020). The future enhancement of the rainfall variability in the
Guinea Coast is associated with an intensification of the mean rainfall.

Heavy rainfalls in West Africa could occur under organized mesoscale convective systems (MCS) such as squall lines, en-
100 hanced convection triggered by the propagation of the African Easterly Waves (AEWs) or moisture advection from the Atlantic
Ocean (Thorncroft and Hoskins, 1994a, b; Gu and Adler, 2004; Maranan et al., 2019; Baidu et al., 2022). A combination of
these different factors could also lead to high impact weather events, such as the very heavy rainfall that occurred in Oua-
gadougou on the 1st of September 2009 (Engel et al., 2017; Lafore et al., 2017; Beucher et al., 2019). More than one third
of the annual rainfall was recorded within 24 hours, and reached 263 mm. In addition, the large-scale sea surface temperature
105 (SST) conditions during this event showed an anomalous warming of the Mediterranean Sea and a negative NAO-like pattern
and a pronounced Atlantic cold tongue. This pronounced cold tongue corresponds to a negative phase of the Atlantic equatorial
mode(AEM), a mode characterized by anomalous warming and cooling in the eastern equatorial Atlantic basin (Zebiak, 1993).
These SST conditions were favourable to an increased rainfall over the Sahel. Another extremely high rainfall event occurred
on the 12th of June 2016 over the Guinea Coast. The rainfall amount recorded in Abakaliki (a station in Nigeria) reached
110 223.5 mm in 24 hours and resulted from a long-lived MCS which was formed over the Darfur elevated areas and then moved
southwestward towards Abakaliki (Maranan et al., 2019).

The first mode of covariability between the sea surface temperature in the tropical Atlantic and the rainfall over West Africa
during the boreal summer indicates a strong connection between the eastern equatorial Atlantic SST and the Guinea Coast
115 rainfall, and explains 31% of the total covariability (Polo et al., 2008). In the current climate, positive phases of the AEM are
characterized by above normal SST conditions in the eastern equatorial Atlantic. The enhanced low-level convergence over the
warm oceanic area is accompanied by an ascent of moist air, which is then advected by the low-level circulation towards the
Guinea Coast. This provides favourable conditions for the rainfall occurrence over this region (Polo et al., 2008; Rodríguez-
Fonseca et al., 2015; Schubert et al., 2016; Lübbecke et al., 2018; Worou et al., 2020, 2022). Over the 1901-2016 period, the
120 eastern equatorial Atlantic positive correlation with the rainfall over the Guinea Coast was stationary during the boreal summer
(Losada et al., 2012; Diatta and Fink, 2014; Worou et al., 2020). Particularly, the decrease in the variance of equatorial Atlantic
SST gradient after 1960s coincides with the decrease in the variance of the rainfall in Guinea Coast (Tokinaga and Xie, 2011).
This highlights the importance of the AEM in driving part of the rainfall variability in the coastal Guinea. Nevertheless, the
variability of the AEM is projected to decrease under future global warming (Worou et al., 2022; Crespo et al., 2022; Yang
125 et al., 2022). This would reduce the Guinea Coast rainfall variability associated with one standard deviation of the AEM. More-
over, over the Guinea Coast, Diatta et al. (2020) showed that the rainfall extremes are strongly correlated with the AEM index.
Atiah et al. (2020) also showed an increase (a decrease) in the total annual wet day rainfall, heavy rainfall and very heavy
rainfall over Ghana during warmer (colder) sea surface conditions in the eastern equatorial Atlantic. Therefore, it is important

to understand and quantify the projected potential changes in the extreme rainfall events in Guinea Coast that are associated
130   with the AEM.

This study aims to further explore the relationship suggested in previous studies between the AEM and the extreme rainfall
events over the Guinea Coast under present-day and future climate conditions by using outputs from CMIP6 models and to
determine how those changes in AEM contribute to the simulated changes in rainfall extremes. The second section is dedicated
135   to the data used in this work and the methods adopted. Section 3 describes the present-day statistics of the rainfall extremes
over the Guinea Coast, and the near-term, mid-term and long-term changes in the mean and variability of these extremes. In
Section 4, the impact of the AEM on the Guinea Coast rainfall extremes under present-day conditions is evaluated, as well as
the future changes in the extreme indices responses related to the AEM. We conclude with the last section, where our findings
are summarized.

2   Datasets and methods

The present study focuses on the impact of the Atlantic equatorial mode on the rainfall extreme events over the Guinea Coast
under different climate conditions. Four 20-year periods are considered: the present-day (1995 - 2014), the near-term future
(2021 - 2040), the mid-term future (2041 - 2060) and the long-term future (2080 - 2099) periods.

2.1   CMIP6 data

145   Rainfalls and SSTs from 24 climate models participating in CMIP6 were retrieved from one of the Earth System Grid Federa-
tion (ESGF) portals (e.g. https://esgf-node.llnl.gov/search/cmip6/, last access: 15 June 2022) and analysed. The analysis for the
present-day period is based on the historical simulations, which covered the 1850-2014 period and were forced with observed
natural and anthropogenic forcings (Eyring et al., 2016). The analyses for the future periods rely on the shared socioeconomic
pathway with a high greenhouse gas emission (SSP5-8.5, O'Neill et al., 2016). These simulations are started from the year
150   2015. We choose the SSP5-8.5 scenario to get the clearest signal of climate change. Only one realization of each simulation is
considered for each GCM. Table 1 provides a list of the different models used and their corresponding ensemble member.

2.2   Observations

Daily rainfall data from the Climate Hazards Group Infrared Precipitation with Station Data (CHIRPS) are used to diagnose the
observed rainfall extremes over West Africa (Survey et al., 2014; Funk et al., 2015). This dataset combines satellite observations
155   with rain-gauge measurements and is available at a spatial resolution of 0.25°. It covers the 1981-2022 period and can be
retrieved from https://data.chc.ucsb.edu/products/CHIRPS-2.0/global_daily/netcdf/p25/ (last access: 16 June 2022). Bichet and
Diedhiou (2018) showed a good quality of the CHIRPS rainfall data when compared to rain gauge data in the Guinea Coast
area. Observed monthly SST data are derived from the Hadley Centre Global Sea Ice and Sea Surface Temperature (HadISST).
This dataset is available at a spatial resolution of 1° (Rayner et al., 2003) and covers the 1870-2022 period.

Table 1. List of the analysed 24 CMIP6 models in this study, as well as their ensemble member considered in the historical and SSP5-8.5 simulations.

CMIP6 model	Historical member	SSP5-8.5 member
ACCESS-CM2	r1i1p1f1	r1i1p1f1
ACCESS-ESM1-5	r1i1p1f1	r1i1p1f1
CESM2	r11i1p1f1	r2i1p1f1
CESM2-WACCM	r1i1p1f1	r1i1p1f1
CNRM-CM6-1	r1i1p1f2	r1i1p1f2
CNRM-CM6-1-HR	r1i1p1f2	r1i1p1f2
CNRM-ESM2-1	r1i1p1f2	r1i1p1f2
CanESM5	r1i1p1f1	r1i1p1f1
EC-Earth3	r1i1p1f1	r1i1p1f1
EC-Earth3-Veg	r1i1p1f1	r1i1p1f1
GFDL-ESM4	r1i1p1f1	r1i1p1f1
HadGEM3-GC31-LL	r1i1p1f3	r1i1p1f3
INM-CM4-8	r1i1p1f1	r1i1p1f1
INM-CM5-0	r1i1p1f1	r1i1p1f1
IPSL-CM6A-LR	r1i1p1f1	r1i1p1f1
KACE-1-0-G	r1i1p1f1	r2i1p1f1
MIROC-ES2L	r1i1p1f2	r1i1p1f2
MIROC6	r1i1p1f1	r1i1p1f1
MPI-ESM1-2-HR	r1i1p1f1	r1i1p1f1
MPI-ESM1-2-LR	r1i1p1f1	r1i1p1f1
MRI-ESM2-0	r1i1p1f1	r1i1p1f1
NorESM2-LM	r1i1p1f1	r1i1p1f1
NorESM2-MM	r1i1p1f1	r1i1p1f1
UKESM1-0-LL	r1i1p1f2	r1i1p1f2

2.3 Methods

This study is focused on the July-September season (JAS), when the Guinea Coast rainfall covariability with the AEM is at its maximum in the current climate models (Worou et al., 2022). This season contributes to $46\,\%$ of the total annual rainfall over the Guinea Coast. It is also dominated by the monsoon system of West Africa, which is characterized by an abrupt shift of the rainfall band from the coastal areas in the end of June to the Sahel region. Sanogo et al. (2022) found a strong coupling between the West African monsoon rainfall and the occurrence of extreme precipitation events, mainly during the boreal summer. The Guinea Coast area extends between $20°W - 15°E$, and $4°S - 10°N$ (similar to Faye and Akinsanola (2021), with 32 points in the selected area on a grid of $2.8\,°{\times}2.8\,°$ resolution.

2.3.1 Definition of the AEM

All the SST data are remapped on a same grid at $1°$ of resolution. Over each 20-year period, the SST data are then linearly detrended at each grid point and averaged over the region between $20°W$ - $0°E$ and $3°S$ - $3°N$. This area is known as the Atlantic Niño (also called AEM or Atlantic zonal mode) region (ATL3, Zebiak, 1993). The obtained monthly SST anomalies are averaged over the JAS season, and then normalized and standardized. This operation is performed for each of the four periods considered.

2.3.2 Computation of the extreme rainfall indices

First, all the daily rainfall data are remapped on the grid of the model which has the lowest resolution ($2.8\,°$). The daily rainfall indices are then computed and averaged over the JAS season. In this work, we analyse a set of 12 rainfall extreme indices defined by the Expert Team on Climate Change Detection and Indices (ETCCDI) (http://etccdi.pacificclimate.org/indices_ def.shtml, last access: 16 June 2022). The details of these indices are provided in Table 2. The indices recommended by the ETCCDI are widely used to monitor and detect changes in drought and wet conditions over different regions. Some applications can be found in several studies such as New et al. (2006); Sillmann et al. (2013a, b); Mouhamed et al. (2013); Diedhiou et al. (2018); Faye and Akinsanola (2021); Delhaye et al. (2022), among others.

2.3.3 Links between the AEM and the extreme rainfall indices

The analysis of the JAS rainfall extreme patterns associated with the JAS AEM is completed through linear regressions of the extreme anomalies at each grid point onto the standardized JAS AEM SST index. The patterns are computed for each GCM and then averaged to obtain the the multi-model ensemble mean (EnsMean). The regression pattern in the observations is computed by regressing the rainfall indices from CHIRPS data onto the standardized AEM index from HADISST. The change in the patterns is defined as the difference of the regression coefficients between the future and present-day periods, and is computed for each GCM. We consider the EnsMean spatial patterns rather than the pattern of each GCM. The reason of this choice is based on the fact that the EnsMean performs better compared to each model, in the representation of the extreme rainfall indices over the West Africa (Akinsanola and Zhou, 2019; Faye and Akinsanola, 2021). For each grid point of the

Table 2. List and definition of the 12 rainfall extreme indices selected for this study.

Index Label	Index Name	Index Definition	Index Unit
SDII	Simple daily intensity index	For each year, compute the average of wet days daily rainfall in the JAS season. A wet day is defined as a day when the rainfall is greater or equal to 1 mm	$mm \cdot day^{-1}$
R10mm	Heavy precipitation days	For each year, count the number of days in the JAS season when the daily rainfall is greater or equal to 10 mm	$days$
R20mm	Very heavy precipitation days	For each year, count the number of days in the JAS season when the daily rainfall is greater or equal to 20 mm	$days$
R95p	Very wet days	Let PR95 be the 95 percentile of the daily rainfall timeseries in the JAS season over the 1995-2014 period (1840 timesteps). For each year, sum of rainfall over days in the JAS season, when the rainfall amount is greater or equal to PR95	mm
R99p	Extremely wet days	Let PR99 be the 99 percentile of the daily rainfall timeseries in the JAS season over the 1995-2014 period (1840 timesteps). For each year, sum of rainfall over days in the JAS season, when the rainfall amount is greater or equal to PR95	mm
R95pf	Precipitation percent due to very wet days	Let PR95 be the 95 percentile of the daily rainfall timeseries in the JAS season over the 1995-2014 period (1840 timesteps). For each year, compute the sum of the daily rainfall greater or equal to PR95 in the JAS season, and divide by the sum of rainfall over all the days in the season. The result is multiplied by 100	%
PRCPTOT	Total wet-day precipitation	For each year, compute the sum of the daily rainfall over wet days of the JAS season. A wet day is defined as a day when the rainfall is greater or equal to 1 mm	mm
RX1day	Maximum 1 day precipitation	For each year, compute the maximum of the daily rainfall over the JAS season	mm
RX5day	Maximum 5 days precipitation	For each year, compute the maximum of the rainfall sum over 5 consecutive days in the JAS season.	mm
CDD	Consecutive dry days	For each year, compute the largest number of consecutive dry days in the JAS season. A dry day is defined as a day when the rainfall is strictly less than 1 mm	$days$
CWD	Consecutive wet days	For each year, compute the largest number of consecutive wet days in the JAS season. A wet day is defined as a day when the rainfall is greater or equal to 1 mm	$days$
FRQW	Frequency of wet days	For each year, compute the number of wet days (when the rainfall is greater or equal to 1 mm) in the JAS season. The result is divided by the total number of days in the JAS season (92), and multiplied by 100	%

EnsMean regression pattern, a signal is considered as robust if 50% of the models present a significant regression coefficient at 5% level and if two thirds of the models agree on the sign of the EnsMean.

2.3.4 Robustness of the mean state changes and of the changes in the teleconnection patterns

A change in the mean state is considered as robust if two thirds of the models show changes greater than the interannual variability (IAV) and two thirds of the models agree on the sign of the change. Similar to Dosio et al. (2021), the IAV is computed for each model following the equation:

$$IAV = \sqrt{\frac{2}{20}} \times 1.645 \times \sigma \tag{1}$$

where σ is the standard deviation of the linearly detrended variable for present-day conditions. The factor $\sqrt{2/20}$ takes into account the variability of the difference between two 20-year periods. The factor 1.645 considers a confidence interval of 90% for the change signal to exceed the IAV. Unrobust change signal is also defined for grid points where more than 80% of the models show a small change compared to their IAV.

For the extreme rainfall regression patterns related to the AEM, a change is considered as robust if more than two thirds of the models agree on the sign of the change (Rehfeld et al., 2020).

2.3.5 Performance metrics for the multi-model EnsMean

The evaluation of the EnsMean performance in representing the spatial distribution of the different extreme indices relative to observations is based on four metrics which have been applied in different studies (e.g., Akinsanola and Zhou, 2019; Faye and Akinsanola, 2021; Akinsanola et al., 2021; Li et al., 2021b) :

  – the percentage of bias (%BIAS)

$$\%BIAS = 100 \times \frac{\sum_{i=1}^{n}(M_i - O_i)}{\sum_{i=1}^{n}O_i} \tag{2}$$

  – the normalized root mean square error (NRMSE)

$$NRMSE = \frac{\sqrt{\frac{1}{n}\sum_{i=1}^{n}(M_i - O_i)^2}}{\frac{1}{n}\sum_{i=1}^{n}O_i} \tag{3}$$

  – the pattern correlation coefficient (PCC)

$$PCC(M,O) = \frac{Cov(M,O)}{\sqrt{Var(M)Var(O)}} \tag{4}$$

  – the Taylor skill score (Taylor, 2001)

$$TSS = \frac{4(1+PCC)^2}{\left(\frac{\sigma_{cmip6}}{\sigma_{observation}} + \frac{\sigma_{observation}}{\sigma_{cmip6}}\right)^2 (1+PCC_0)} \tag{5}$$

where M and O are model and observation values, respectively, i is the index of a grid point, n is the number of grid points over which the data are compared, Cov and Var are the covariance and variance, respectively, PCC_0 is the maximum correlation reachable, set to 1 in our case, and σ_{cmip6} and $\sigma_{observation}$ are the standard deviations of the EnsMean and observations

220 patterns (mean state patterns or teleconnection patterns) over the Guinea Coast, respectively. TSS and PCC ($\%BIAS$ and $NRMSE$) values are close to one (zero) for a very good representation of the observations by the models' EnsMean. The TSS is close to zero for no match between the EnsMean and observations.

3 Present and future rainfall extremes over the Guinea Coast

3.1 Mean JAS rainfall extremes in Guinea Coast under present-day conditions

225 First, we present the JAS spatial distribution of the rainfall extremes simulated by climate models over West Africa in the present-day period (Fig. 1). Most of the indices show maximum values over the Guinean Highlands (in the western Guinea Coast) and the Cameroon mountains (east of $5°E$), and moderate values in the center Guinea Coast (between $7.5°W$ and $5°E$). From $10°N$ to the North, there is a gradual decrease (increase) of the wet (dry) indices. In particular, the total precipitation over wet days (PRCPTOT) ranges between 600 and $1000\,\mathrm{mm}$ (200 and $800\,\mathrm{mm}$) over the center Guinea Coast in the EnsMean

230 (observations). Except for R95pf and RX1day, the EnsMean captures reasonably well the spatial distribution of the rainfall extremes over the Guinea Coast. However, there are some biases in the EnsMean, relative to the observations (Fig. 2, Fig. A1). In particular, a dominant positive (negative) bias in CWD and FRQW (CDD) is present over the entire Guinea Coast. For SDII, R95pf and RX1day, the biases are negative along the coast and positive more inland. For the other indices, most of the biases are positive in the center of the Guinea Coast and negative elsewhere in the region.

235

Table 3 illustrates the performance of the models in simulating the mean JAS rainfall-based extreme indices by comparing the Guinea Coast grid point values in the EnsMean against the observations. The R10mm and the PRCPTOT are the variables that are the best represented by the EnsMean, as indicated by the Taylor skill score values of 0.77 and 0.70, respectively. R20mm, PRCPTOT and R10mm exhibit the highest pattern correlation coefficients, which amount to 0.93, 0.91 and 0.84, re-

240 spectively. Only R95pf and RX1day present a PCC value below 0.5. These variables also present the poorest Taylor Skill Score (0.14 and 0.19, respectively). Moreover, the R95pf, R10mm and PRCPTOT root mean square error represents 25%, 27% and 27% of the mean observed values, respectively, which are the lowest among the different variables considered. Furthermore, there are too many consecutive wet days in the climate models compared to observations, while the number of consecutive dry days is too low. The CWD exhibits the highest percentage bias (+72.99%) relative to observations. This overestimation of the

245 CWD by the GCMs over the coastal regions has been reported by Faye and Akinsanola (2021). Likewise, the frequency of wet days present a positive bias in the EnsMean that amounts to 18.09% of the observations.

The maximum rainfall over 5 consecutive wet days (RX5day) is better represented than the maximum one-day rainfall (RX1day). Its pattern correlation coefficient amounts to 0.75, and the Taylor skill score equals 0.47. The EnsMean overesti-

mates the overall RX5day over the Guinea Coast, and the percentage of bias reaches 0.98%, against -1.28% for RX1day. Alongside, the wet days and extremely wet days (R95p and R99p) statistics over the entire Guinea Coast show positive biases that represent 14.66% and 24.10% of the observations, respectively (0.36 and 0.44 for their NRMSE). Furthermore, the Taylor skill score of the fraction of wet days rainfall that contributes to the seasonal rainfall (R95pf) is very poor (around 0.14). Next, we will describe the changes of the rainfall extremes over the Guinea Coast under global warming, as projected by the climate models. All the indices will be studied, regardless of their good or poor representation by the GCMs.
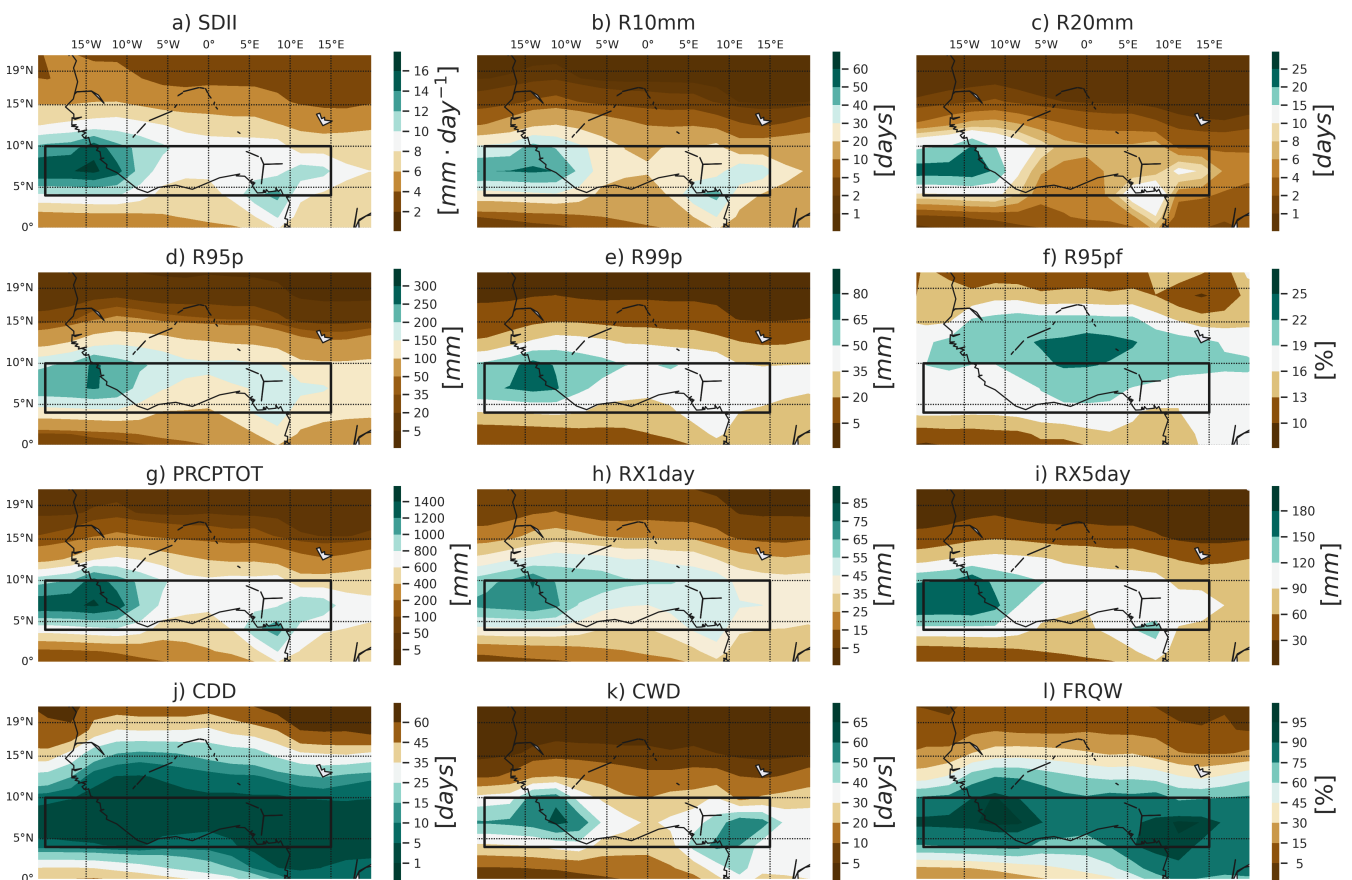
Figure 1. EnsMean distribution of the mean JAS extreme rainfall indices over the 1995-2014 period from 24 CMIP6 models. The black rectangles indicate the Guinea Coast region.

3.2 Changes in the mean and variability of the JAS rainfall extremes over the Guinea Coast

Figure 3 displays the projected EnsMean long-term changes (2080-2099 minus 1995-2014) in the rainfall extreme indices over West Africa. The spatial patterns of the changes (relative to the present-day period) in the extreme rainfall indices over West Africa are similar for the near-term, mid-term and long-term periods, with, in general, a gradual increase in magnitude over
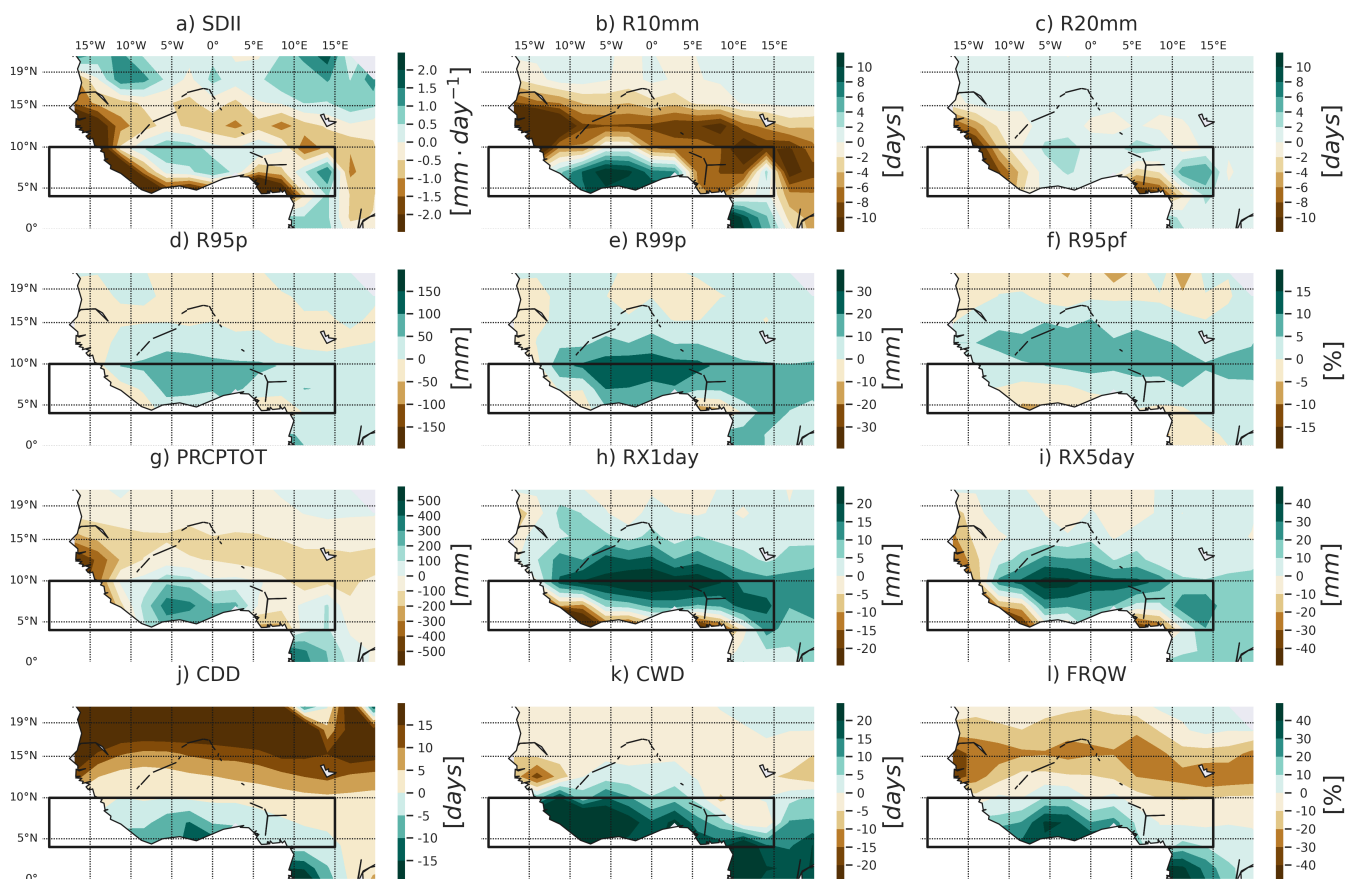
Figure 2. Spatial distribution of the EnsMean bias relative to CHIRPS for the JAS mean of the 12 rainfall-based extreme indices over the 1995-2014 period. The black rectangles indicate the Guinea Coast region.

260   the three future periods. The total wet day precipitation (PRCPTOT) is projected to increase (decrease) significantly over the eastern (western) Sahel (Fig. 3 (g)). Over the Guinea Coast, the change in PRCPTOT is weaker and not robust, compared to the changes over the Sahel. The spatial distribution of the JAS PRCPTOT mean change over West-Africa is similar to the change in the mean June-August (JJA) rainfall obtained in early studies by Dosio et al. (2021), as well as the change in the wet season rainfall obtained by Wainwright et al. (2021). Moreover, the intensity of the daily rainfall over wet days (SDII)

265   increases significantly in most areas of the Guinea Coast (Fig. 3 (a)), and the frequency of wet days significantly decreases (Fig. 3 (i)). Additionally, the maximum consecutive wet day (CWD) indices are projected to decrease over the Guinea Coast and the western Sahel. For the maximum consecutive dry days (CDD), there is a projected significant decrease (increase) in the eastern (western) Sahel, while over the Guinea Coast, there is an insignificant increase in the CDD. The change pattern in the CDD index is consistent with findings by Dosio et al. (2021). These changes in CWD and CDD also confirm the findings

270   of Klutse et al. (2018) under a global warming of $1.5\,°C$ and $2\,°C$. Consistently, Wainwright et al. (2021) found an increase (a

Table 3. Performance of the multi-model ensemble mean in representing the spatial distribution of the rainfall extreme indices over the Guinea Coast.

	%BIAS	NRMSE	PCC	TSS
SDII	-19.22	0.50	0.58	0.25
R10mm	-3.71	0.27	0.84	0.77
R20mm	-16.16	0.51	0.93	0.63
R95p	14.66	0.36	0.78	0.62
R99p	24.10	0.44	0.70	0.56
R95pf	8.59	0.25	-0.14	0.14
PRCPTOT	0.53	0.27	0.91	0.70
RX1day	-1.28	0.53	0.29	0.19
RX5day	0.98	0.34	0.75	0.47
CDD	-46.35	0.92	0.68	0.20
CWD	72.99	0.92	0.62	0.65
FRQW	18.09	0.30	0.64	0.31

decrease) in the mean length of dry (wet) spells over the Guinea Coast during the wet season in a future warmer climate. There is also a robust increase in the maximum 1 day and maximum 5 consecutive days precipitation (RX1day and RX5day) over the Sahel and Guinea Coast. These results show a tendency to less frequent and more intense rainfall over the Guinea Coast in a warmer climate, which happens over shorter duration. Our results are in accordance with Dosio et al. (2021), who found an

275 increase in the mean SDII, RX1day and a decrease in the number of wet days in the JJA long-term projections for the Guinea Coast.

The assessment of the changes in the very wet days and extremely wet days indices (R95p and R99p) confirms an enhancement of the extreme rainfall events in the Guinea Coast, which is however unrobust. The contribution of the wet days rainfall

280 to the total seasonal rainfall (R95pf) also increases over the majority of West Africa, with a low confidence. Events of rainfall exceeding $10\,\mathrm{mm}$ and $20\,\mathrm{mm}$ (R10mm and R20mm indices) are reinforced between $5°\,W$ and $10°\,E$, with only few significant signals over the Guinea Coast. The spatial distribution of the mean changes in R95p, R10mm and R20mm in our study are different from the patterns obtained in the RCM-CMIP5 projections (Akinsanola and Zhou, 2019).

285 Figure 4 displays the average of the change in mean and standard deviation of the extreme rainfall indices over the Guinea Coast for the 2021-2040, 2041-2060 and 2080-2099 periods, relative to 1995-2014. There is a large uncertainty around the change in the mean total wet-day precipitation (PRCPTOT) over the Guinea Coast in the three future periods, while an increase in the total wet-day rainfall variability is obtained in the mid-term and long-term future periods. Except the R10mm, CDD and FRQW, the magnitude of the change in both the mean and standard deviation gradually increases with time over the
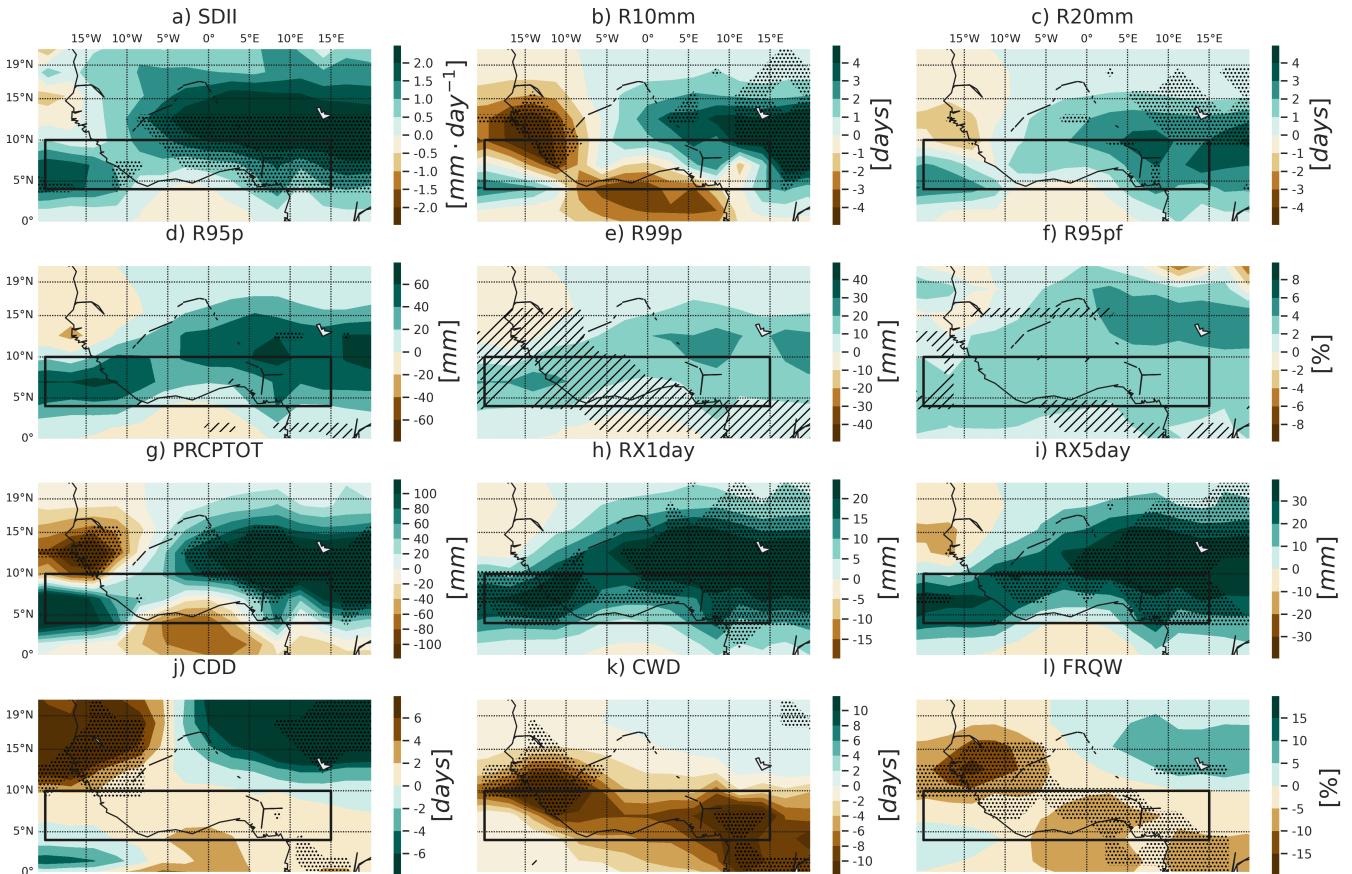
Figure 3. Projected multi-model ensemble mean long-term change in the JAS rainfall extreme indices over West Africa, relative to the present-day period (2080-2099 minus 1995-2014). The stippling indicates grid points where two thirds of the models show changes greater than the interannual variability and two thirds of the models agree on the sign of the change. Diagonal bars show areas where the change is weaker than the interannual variability.

three future periods. The changes in the near-term period relative to the present-day conditions are not clear for the majority of the indices. The mid-term and long-term changes indicate a clear increase in mean and standard deviation of the simple daily rainfall intensity, the very wet days and extremely wet days, as well as the contribution of very wet days to the seasonal total rainfall. The maximum 1 day and 5 days precipitation also increases clearly in mean and standard deviation over the mid-term and long-term periods, relative to the present-day period. Besides, the mean and variability of the CDD index increase, while they decrease for the CWD index in the mid-term and long-term periods, relative to the present-day period. The frequency of wet days is reduced in mean, with little changes in its variability. These results suggest a decrease in frequency of rainfall events and an intensification of extreme rainfall events over shorter days over the Guinea Coast in the middle and the end of the 21st century, under the highest emission greenhouse gas scenario. The projected long-term increase (decrease) in the mean
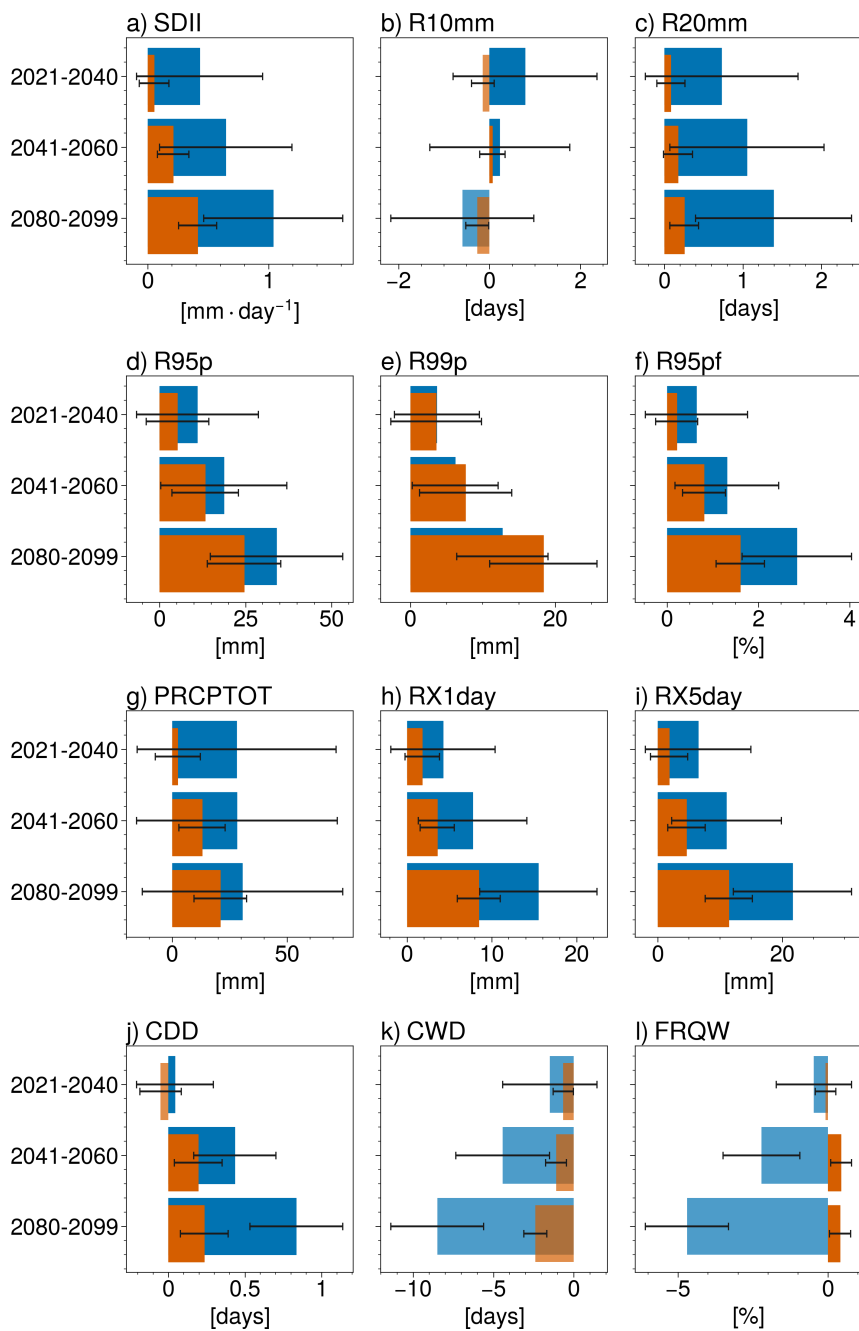
Figure 4. Average of the near-term, mid-term and long-term changes (relative to the present-day period) in the mean and standard deviation of the rainfall extreme indices over the Guinea Coast. Positive (negative) changes in the mean are highlighted with a blue (cyan) colour. Positive (negative) changes in the standard deviation are drawn in orange (brown). Black horizontal bars indicate the 90% confidence interval of the difference in the mean over the 24 models.

of SDII, R20mm, R95p, RX5day (CWD) averaged over the Guinea Coast are in accordance with Akinsanola and Zhou (2019),
300   as well as the increase in CDD from the central to eastern Guinea Coast.

In summary, under future global warming, rainfall events over the Guinea Coast are projected to intensify (increase in the
daily rainfall intensity over wet days), to be less frequent, to happen over shorter days, and to be more extreme (increase in the
amount of rainfall during very wet and extremely wet days). Moreover, there is a projected increase in the variability of most
305   of the rainfall-based extreme indices, which is consistent with Akinsanola et al. (2020). The multi-model median long-term
percentage of change in mean and variability averaged over the 12 indices amounts to $10.46\,\%$ and $16.44\,\%$, respectively. Wet
and dry extreme events in the Guinea Coast could also happen under positive or negative phases of the Atlantic equatorial
mode. Thus, it is important to understand the future changes in the rainfall extremes indices over the Guinea Coast that are
connected with the AEM.

310   ## 4   Impact of the AEM on the rainfall extreme events over the Guinea Coast

The impact of the AEM on the extreme rainfall variability during the boreal summer is assessed by regressing the JAS extreme
indices onto the standardized JAS AEM index.

4.1   AEM impact on the rainfall extreme events under present-day climate conditions

Except for the total wet-day precipitation index, the regression coefficients of the EnsMean for the extreme indices are hardly
315   significant over the Guinea Coast and the entire West Africa. Most of the significant signals are located in the Atlantic oceanic
region. The EnsMean regression patterns associated with one standard deviation of the AEM index show an increased intensity
of rainfall over wet days (SDII) (0.2 to $0.6\ mm \cdot day^{-1}$) and total wet-day rainfall (up to $60\,\mathrm{mm}$) over the Guinea Coast (Fig.
5(a),(g)). The number of days with heavy and very heavy precipitation (R10mm and R20mm) are also increased up to three
days and one day, respectively, during positive AEM events (Fig. 5(b)-(c)). Table 4 displays the performance metrics of the
320   extreme rainfall indices related to the AEM. Compared to the observations, there is overall a good spatial distribution of the
SDII and PRCPTOT anomalies over West Africa (Fig. A2). Over the Guinea Coast, the SDII and PRCPTOT pattern correla-
tion coefficients between the EnsMean and observations are 0.74 and 0.52, respectively . In addition, PRCPTOT presents the
best skill score among the different indices (0.56), and one of the lowest NRMSE (0.81). For R10mm and R20mm, the PCC
values amount to 0.48 and 0.51, respectively. Nonetheless, over the Guinea Coast, the SDII, PRCPTOT, R10mm and R20mm
325   responses to AEM are underestimated in the EnsMean, compared to the observations (Table 4, Fig. 6).

Warmer than average sea surface conditions in the eastern equatorial Atlantic favour an increased amount of rainfall during
very wet and extremely wet days, as well as the contribution of the very wet days to the seasonal total rainfall (Fig. 5(d)-(f)).
Over the Guinea Coast, the anomalies related to one standard deviation of the AEM index range between 10 and $30\,\mathrm{mm}$ for
330   R95p. The contribution of the wet days rainfall to the seasonal rainfall is increased up to 3%. For R99p, the anomalies are
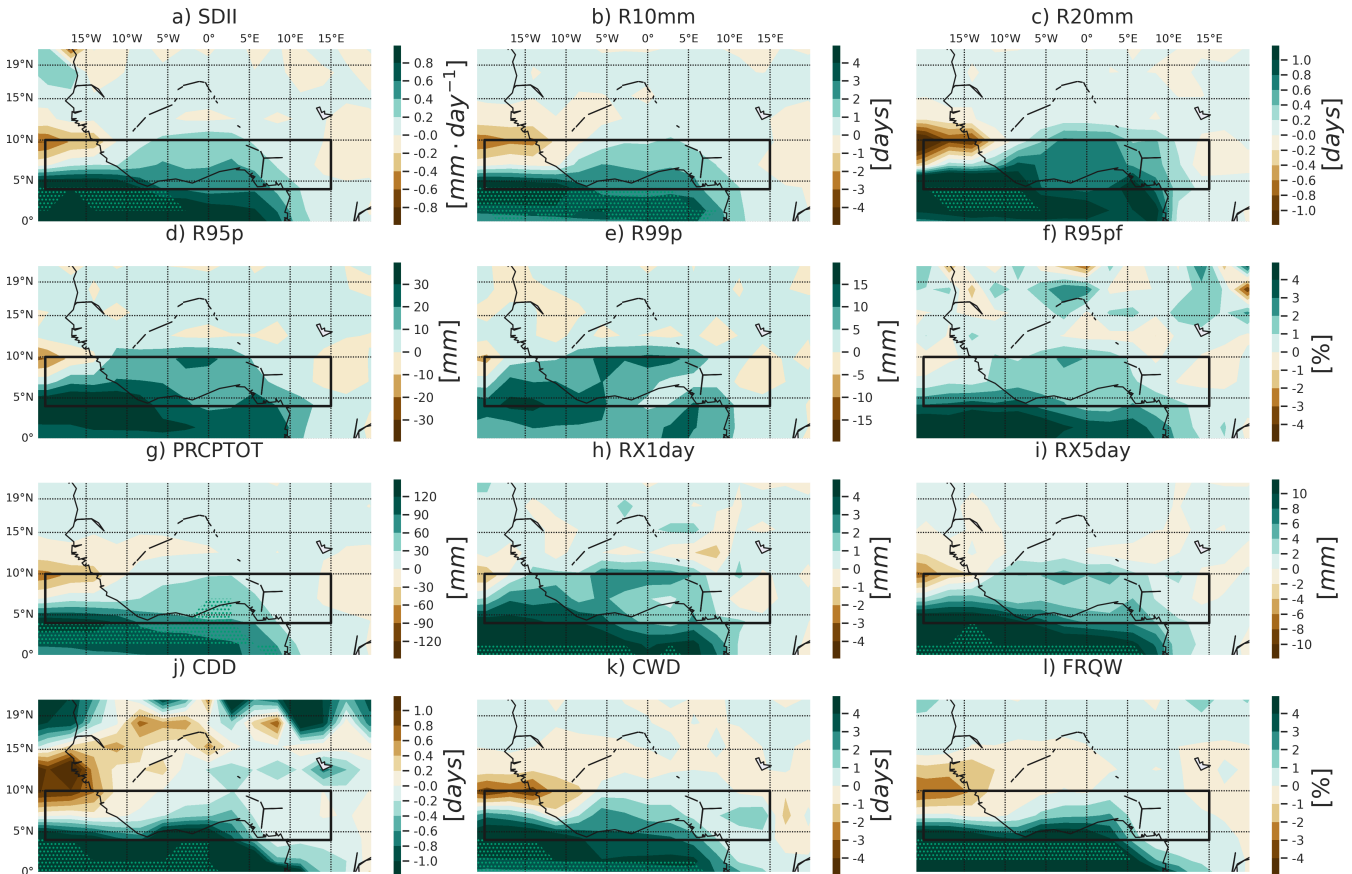
Figure 5. Maps of the JAS rainfall extreme indices regressed onto the standardized JAS AEM SST index over the 1995-2014 period. The stippling represents grid points where 50% of the models show a significant regression coefficient at 5% level and where two thirds of the models agree on the sign of the regression coefficient. The black rectangles indicate the Guinea Coast region.

between 5 and 15 mm (0 to 10 mm) in most areas located to the west (east) of 5°E. Although the regression patterns of R95p, R99p and R95pf are positively correlated with the observed patterns, their skill scores are weak (between 0.18 and 0.26). Compared to the observations, the regression patterns of R99p and R95pf in the EnsMean for the Guinea Coast present some positive biases which are the strongest among the different indices (Table 4, Fig. 6 (e)-(f)). For R95p, the regression pattern in the EnsMean is underestimated compared to the observations, mainly along the western coast (Fig. 6(d)).

335

The maximum daily precipitation and the maximum precipitation over five consecutive days (RX1day and RX5day) are intensified over the Guinea Coast during warm phases of the AEM (Fig. 5(h)-(i)). The increase in RX1day reaches 3 mm, against 2 to 6 mm for RX5day. The RX1day regression coefficients are overestimated in EnsMean compared to the observations, with a

340 bias percentage of 41.99 %. This index also has a weak Taylor skill score (0.15) while its pattern correlation between EnsMean

and observation amounts to 0.48. Unlike the response of RX1day to the AEM phases, the magnitude of the RX5day anomalous pattern is lower in EnsMean than observed. The bias percentage is -9.16%. Besides, the RX5day PCC and TSS values are weak (0.41 and 0.28, respectively).

Table 4. Performance of the EnsMean in simulating the JAS Guinea Coast rainfall extremes regression patterns associated with the AEM over 1995-2014.

	%BIAS	NRMSE	PCC	TSS
SDII	-54.42	0.97	0.74	0.42
R10mm	-53.64	0.81	0.48	0.53
R20mm	-49.84	1.07	0.51	0.41
R95p	-2.96	1.43	0.27	0.26
R99p	350.11	9.17	0.35	0.18
R95pf	1199.96	21.78	0.19	0.26
PRCPTOT	-55.36	0.81	0.52	0.56
RX1day	41.99	3.45	0.48	0.15
RX5day	-9.16	1.65	0.41	0.28
CDD	-50.87	-1.58	0.13	0.32
CWD	-50.86	1.72	-0.39	0.09
FRQW	-63.87	1.10	0.18	0.34

345 The anomalous EnsMean patterns of the maximum consecutive dry and wet days related to a warm phase of the AEM show a reduction in the length of dry spells over the Guinea Coast, and an increase in wet spells duration (Fig. 5(j)-(k)). The decrease in CDD is less than one day and the overall distribution of CDD in the Guinea Coast is underestimated. The bias percentage amounts to -50.87%, and the pattern correlation coefficient with observations is close to zero. For the CWD index, the EnsMean pattern indicates an increase of one to three days in its values over coastal areas during positive AEM phases.

350 However, there is a negative correlation between the EnsMean pattern and the observations pattern for this index (-0.39). The CWD response to the AEM in the EnsMean has the poorest Taylor skill score over the Guinea Coast (Table 4). Similarly, the frequency of wet days over the Guinea Coast is amplified up to 4% under warm sea surface conditions in the eastern equatorial Atlantic. Compared with the observations, the FRQW anomalous values are also underestimated in the EnsMean, with a bias percentage of -63.87%. The FRQW pattern correlation between the EnsMean and observations is weak, and the TSS is equal

355 to 0.34.

In summary, the warming of the eastern equatorial Atlantic during positive phases of the AEM leads to positive (negative) anomalies in the wet (dry) extreme indices over the Guinea Coast. This result is consistent with Atiah et al. (2020); Diatta et al. (2020). However, according to the Taylor skill score, the performance of the models in representing the anomalous responses

360 in the different extreme indices is poor to modest, although some indices exhibit a good pattern correlation coefficient. In the next section, the future changes in the Guinea Coast extreme rainfall indices related to the AEM will be assessed.
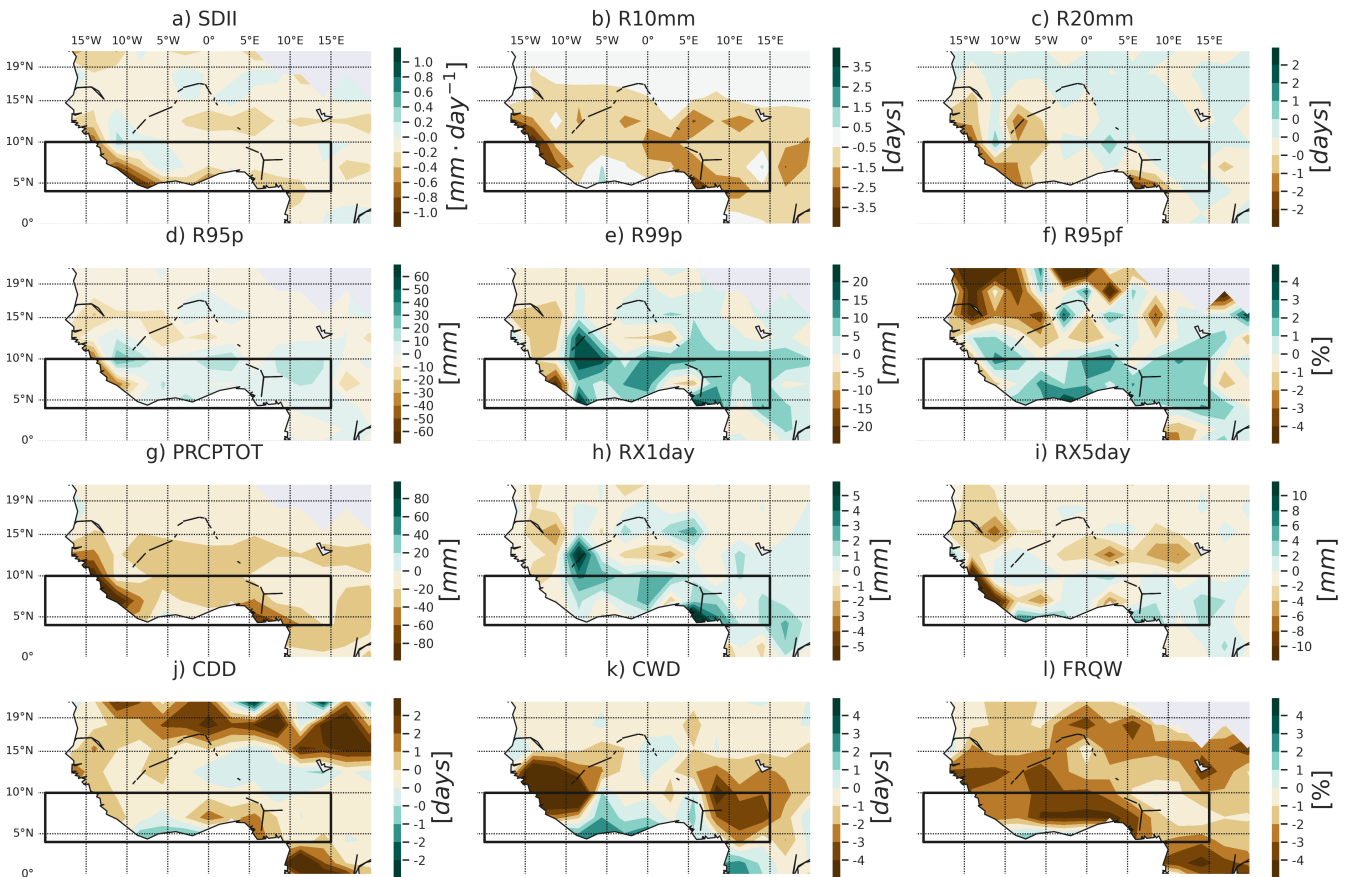
Figure 6. Spatial distribution of the EnsMean bias relative to observations for the JAS regression pattern of the extreme rainfall indices related to one standard deviation of the Atlantic equatorial mode. The black rectangles indicate the Guinea Coast region.

4.2 Future changes in the rainfall extreme events associated with the AEM

The changes of the equatorial Atlantic mean state under the highest greenhouse gas emission scenario (SSP5-8.5) lead to a weakened variability of the AEM in the future (Worou et al., 2022; Crespo et al., 2022; Yang et al., 2022). Worou et al. (2022)

365 showed a projected weakening of the trade winds climatology over the equatorial Atlantic and a deeper thermocline in the eastern equatorial Atlantic which would lead to a reduction of the coupling between the surface and the thermocline depth. This implies a future weakening of the Bjerknes feedback (Bjerknes, 1969) in the equatorial Atlantic that explains the reduced variability of the AEM under global warming, and the weaker future impact of the AEM on the rainfall over the equatorial Atlantic and the Guinea Coast. These results are confirmed by Crespo et al. (2022), who found a future reduction of the AEM

370 variability in a warmer climate, mainly due to a weakening of the third component of the Bjerknes feedback (the SST response
to the variations of the thermocline depth). Yang et al. (2022) also found a reduced AEM variability. They underlined a greater
role of a more stable tropical Atlantic atmosphere background in a future warmer climate (Jia et al., 2019), in reducing the
AEM variability, compared to the weakening associated with the deepening of the eastern equatorial Atlantic thermocline. Sub-
sequently, the variability of the JAS rainfall over the equatorial Atlantic and Guinea Coast that is related to the different phases
375 of AEM is reduced (Worou et al., 2022). Figure 7(g) shows a clear decrease in the variability of the total wet-day precipitation
averaged over the Guinea Coast, which is associated with one standard deviation of the AEM in the near-term, mid-term and
long-term future periods, compared to the present-day situation. This result is in accordance with Worou et al. (2022). The
EnsMean change in the PRCPTOT response to AEM amounts to -6.7, -10.8 and $-15\,\mathrm{mm} \cdot \mathrm{days}^{-1}$ for the consecutive three
future periods. The models' median reduction percentage in the PRCPTOT-AEM values compared to the 1995-2014 period
380 are -31%, -33% and -50% for the near-term, mid-term and long-term future periods, respectively. The spatial distribution
of the long-term change in the PRCPTOT-AEM values over the Guinea Coast ranges between -10 and $-30\,\mathrm{mm}$ (Fig. 8(g)) in
most of the areas located westward of $5°E$.

The variability of the simple daily rainfall intensity in relation with the AEM is reduced in a warmer climate, compared to the
385 present-day conditions. The magnitude of the change in the Guinea Coast SDII-AEM EnsMean ranges from $-0.09\,\mathrm{mm} \cdot \mathrm{day}^{-1}$
in 2021-2040 to $-0.17\,\mathrm{mm} \cdot \mathrm{day}^{-1}$ in 2080-2099 (Fig. 7(a)). The models' median values of the percentage of change in the
regression coefficients averaged over the Guinea Coast are -20%, -30% and -40% in the near-term, mid-term and long-term
periods, respectively. The spatial distribution of the long-term change in the SDII over the Guinea Coast gives values that reach
$-0.4\,\mathrm{mm} \cdot \mathrm{day}^{-1}$, which are barely robust over the region (Fig. 8(a)).

390

The number of days with heavy and very heavy precipitation associated with one standard deviation of the AEM also de-
creases in the future periods compared to the present-day period (Fig. 8(b)-(c)). The average of the R10mm (R20mm) changes
relative to 1995-2014 over the Guinea Coast equals $-0.28(-0.18)$, $-0.29(-0.22)$ and $-0.61(-0.33)$ $days$ in the 2021-2040,
2041-2060, 2080-2099 periods, respectively (Fig. 7 (b)-(c)). The multi-model median values corresponding to the percentage
395 of changes in the area averaged R10mm (R20mm) regression coefficients over the Guinea Coast lie between -28% and -72%
(-37% and -86%) over the three future periods.

The spatial patterns of the future changes in the variability of rainfall during the very wet days and extremely wet days (R95p
and R99p) that is related to the warm and cold AEM events indicate a reduction in R95p and R99p magnitudes over most of the
400 areas in the west of $5°E$ in the Guinea Coast (Fig. 8(d)-(e)). The spatial change patterns are similar for both variables, and very
few grid points agree on the sign of the change across the different models. The EnsMean change in the R95p (R99p) averaged
over the Guinea Coast ranges from $-6.57\,\mathrm{mm}$ to $-8.79\,\mathrm{mm}$ ($-2.43\,\mathrm{mm}$ to $-3.76\,\mathrm{mm}$) over the three future periods (Fig.
7(d)-(e)). The multi-model median values of the Guinea Coast R95p (R99p) change percentage reaches -34% (-44%), -42%
(-45%) and -49% (-26%) in the near-term, mid-term and long-term future periods, respectively, relative to the present-day
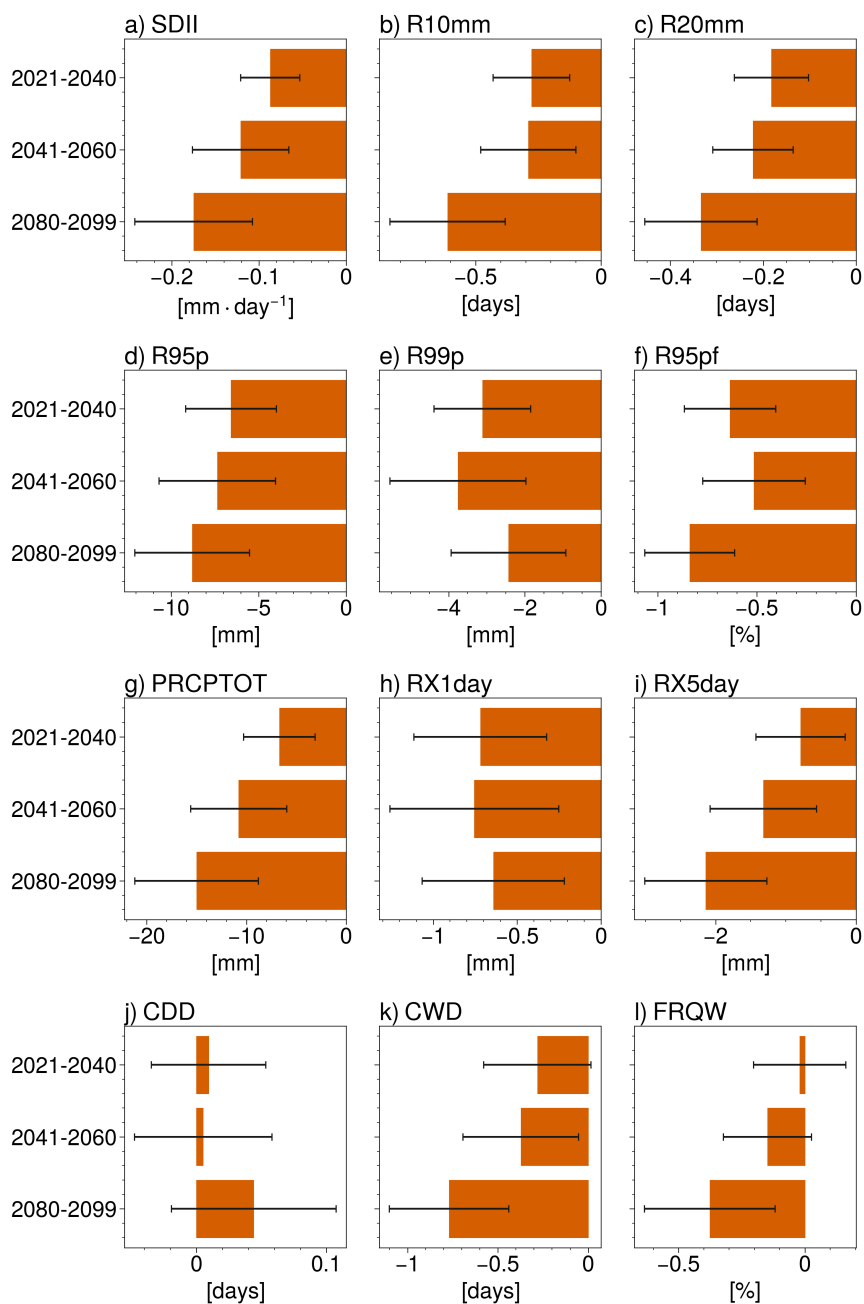
Figure 7. Near-term, mid-term and long-term changes in the average of the JAS extreme rainfall responses to one standard deviation of the JAS AEM index over the Guinea Coast. Black bars indicate the 90% confidence interval of difference in the mean over 24 GCMs.

period. In addition, the anomalous contribution of the very wet day precipitation to the total seasonal rainfall also weakens (Fig. 7(f) and Fig. 8(f)). The average of the R95pf-AEM change over the Guinea Coast ranges between $-0.51\,\%$ and $-0.84\,\%$, and the median percentage of change of the R95pf-AEM lies between -34% and -46% for the three future periods.
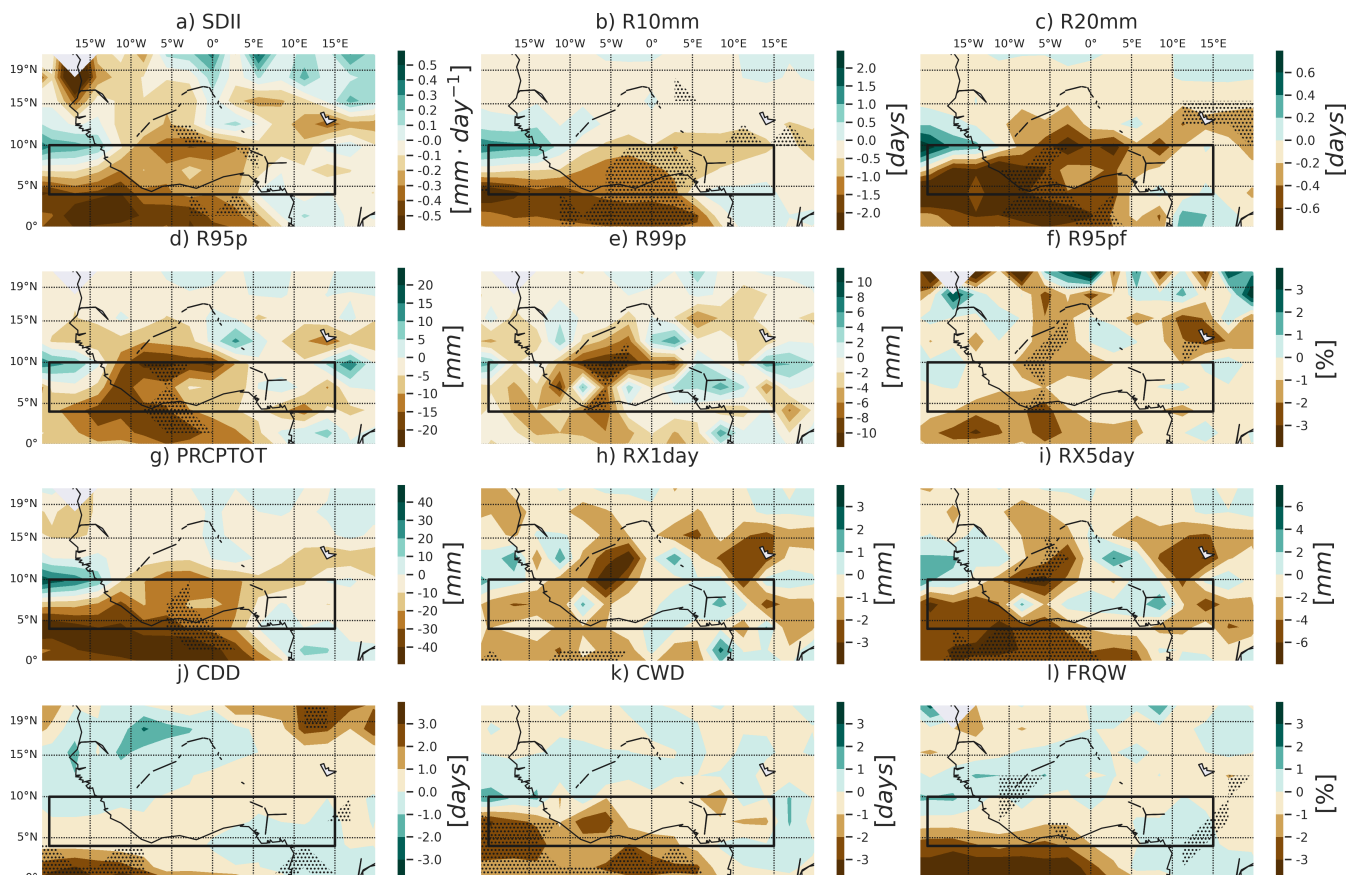
Figure 8. Long-term changes in the regression patterns of the JAS extreme rainfall indices associated with the standardized JAS AEM SST index (2080-2099 minus 1995-2014). The stippling indicates grid points where two thirds of the models agree on the sign of the change.

Lower maximum one day and maximum five days precipitation related to one standard deviation of the AEM index averaged over the Guinea Coast are projected in the 2021-2040, 2041-2060 and 2080-2099 periods, compared to their magnitude in the 1995-2014 period (Fig. 7(h)-(i)). Over the three future periods, the EnsMean reduction is lower than $1\,\mathrm{mm}$ for the RX1day index, while the decrease is between -0.79 and $-2.14\,\mathrm{mm}$ for RX5day. Besides, the multi-model median values of the percentage of change in the RX1day (RX5day) averaged over the Guinea Coast range between -7% and -68% (-20% and -55%) for the three future periods. The maps of the changes in the RX1day and RX5day responses to AEM events are similar (Fig. 8(h)-(i)). The sign of the change is not uniform over the Guinea Coast, and the models hardly agree on the change sign

over the grid points.

The projected decrease in the AEM variability in the future leads to a decrease in the magnitude of the wet and dry spells corresponding to one standard deviation of the AEM index. However, the EnsMean change in the anomalous responses of

420 these indices averaged over the Guinea Coast is less than one day in the different three future periods (Fig. 7(j)-(k)). For the long-term change particularly, the reduction is clear for CWD, while for CDD, the 90% confidence interval indicates that the EnsMean change ranges between -0.02 and 0.1 days. For the other periods, there is a weak confidence around the sign of the change. In addition, the multi-model median value of the change percentages of the CDD (CWD) averaged over the Guinea Coast approximate $-32\%(-54\%)$, $-24\%(-45\%)$ and $-50\%(-82\%)$ for the near-term, mid-term and long-term future pe-

425 riods, relative to the present-day period. Figure 8(j)-(k) displays the spatial distribution of the long-term changes of the two indices. It shows an overall decrease in the CDD and CWD magnitudes over the Guinea Coast, which are between zero and one day for CDD and reaches three days in the west of $5°W$ in the Guinea Coast for CWD. For both indices, there is no grid point in which more than two thirds of the models agree on the sign of the change over the Guinea Coast.

430 Finally, a reduction in the positive anomalies of the frequency of wet days over the Guinea Coast that are linked with one standard deviation of the AEM is projected in the future, under the SSP5-8.5 scenario. The grid-point values of the long-term change pattern are between 0 and -2%. There are only few areas in the Guinea Coast where models agree on the long-term reduction (Fig. 8(l)). The averages of the change patterns over the Guinea Coast are equal to -0.02%, -0.15% and -0.38%, for the three consecutive future periods, respectively, relative to the present-day period (Fig. 7(l)). The multi-model median

435 value of the percentage of the change in the FRQW-AEM index averaged over the Guinea Coast ranges between -17% and -50% over the three future periods.

Table 5 shows the multi-model median value of the part of the variance explained by the AEM for the 12 rainfall-based extreme indices in each of the four periods. For each of the extreme indices, there a a clear decrease of the proportion of

440 variability explained by the AEM in the three future periods, compared to the present-day. Moreover, the reduction is stronger in the long-term period for the majority of the indices (except for the CWD). Under the present-day conditions, the AEM variability explains between 12.51% and 27.74% of the variance of the extreme indices over the Guinea Coast. In the 2080-2099, the proportion of variance explained by the AEM lies between 4.25% and 12.18% across the different variables. The corresponding multi-model median value of the percentage of change relative to 1995-2014 ranges between $-8.25\,\%$ and $-64.97\,\%$.

445

In summary, subsequent to the decrease in the AEM variability in a future warmer climate relative to the present-day conditions, there is a decrease in the variability of the extreme rainfall indices associated with the AEM. Crespo et al. (2022) demonstrated that the models with the strongest warm sea surface biases exhibit the weakest change in both the AEM variability and the third component of the Bjerknes feedback. Given the positive SST biases in most of the CMIP6 models in the eastern

450 Atlantic basin (Richter and Tokinaga, 2020; Worou et al., 2022; Crespo et al., 2022), improving these biases would likely

increase the change in the AEM variability, suggesting that the projected weakened AEM variability is robust despite these biases. Moreover, despite the increase in the total variability of the majority of the extreme indices under global warming in the future (Section 3.2), there is a reduction of the proportion of variance explained by the AEM for these extreme indices. This result highlights a weaker role played by the AEM in the future, in explaining the rainfall extreme variability over the Guinea

455   Coast. Furthermore, there is more confidence in the results averaged over the Guinea Coast than in the spatial distribution of the changes in the teleconnection patterns.

Table 5. Rainfall extreme indices averaged over the Guinea Coast: multi-model median values of the proportion of the variance explained by the AEM over four different periods (in %).

	1995-2014	2021-2040	2041-2060	2080-2099
SDII	23.26	12.33	17.25	5.13
R10mm	27.74	15.62	19.95	12.18
R20mm	15.94	8.02	10.85	5.34
R95p	16.44	10.21	12.79	7.42
R99p	15.91	8.16	9.97	6.12
R95pf	15.05	9.32	13.58	4.60
PRCPTOT	23.30	17.03	19.18	10.47
RX1day	12.51	8.87	13.38	4.25
RX5day	20.33	11.95	17.46	9.17
CDD	13.11	10.19	11.88	7.41
CWD	13.47	6.59	9.96	6.17
FRQW	26.35	18.43	16.75	5.85

5   Summary and conclusions

In this study, the performance of 24 GCMs participating in CMIP6 in simulating 12 JAS rainfall-based climate extremes indices over the Guinea Coast was assessed as well as the projected mean changes in these extremes under global warming. The

460   EnsMean simulates less intense but too frequent rainfall over the Guinea Coast, compared to the observations. The duration of the wet (dry) spells are also longer (shorter) in the EnsMean compared to CHIRPS. There is a need to improve the GCMs for a better representation of the mean state of the West African hydroclimate. This would lead to a more reliable use of climate models for climate services over West Africa, in order to implement better mitigation and adaptation strategies to climate change. Despite the biases, the mean extreme indices show an overall good spatial pattern correlation between the EnsMean

465   and CHIRPS over the Guinea Coast region. The PCC values range between 0.58 and 0.93 for 10 indices over 12.

Under the SSP5-8.5 scenario, changes in the near-term (2021-2040), mid-term (2041-2060) and long-term (2080-2099) periods are evaluated, relative to the present-day climate conditions (1995-2014). Consistent with previous studies (Dosio et al., 2021; Wainwright et al., 2021), results of the average of the mean changes in the extreme indices over the Guinea Coast indicate an intensification of the daily rainfall, together with a decrease in the frequency of wet days and the duration of wet spells. In parallel, the length of the dry spells increases. The number of days with precipitation exceeding 20 mm is modestly increased, while the rainfall amount during the very wet days and extremely wet days is enhanced. Similarly, the maximum rainfall amount over one day and five consecutive days intensifies.

The sign of the long-term change in R10mm and PRCPTOT is not uniform over the Guinea Coast, unlike the sign of the changes in the other extreme indices. The PRCPTOT increases in the west of $5°W$, in the northern part of the Guinea Coast and in the east of $5°E$, while it decreases in the other areas of the Guinea Coast. Moreover, except for R10mm, CDD, CWD and FRQW, there is a gradual increase with time in the variability of the different extremes indices averaged over the Guinea Coast, for the consecutive three future periods.

Anomalous warming (cooling) of the eastern equatorial Atlantic in positive (negative) phases of the AEM is associated with increased (decreased) total rainfall over the Guinea Coast in the current climate. Our results indicate, on the one hand, an in-phase relationship between the wet extreme indices of the Guinea Coast and the AEM SST index. A positive AEM phase is also accompanied by a decrease in the CDD. However, the multi-model EnsMean spatial distributions of the extreme rainfall anomalies related to one standard deviation of the AEM under the present-day conditions are barely significant over the Guinea Coast.

On the other hand, there is a projected weakening of the AEM under global warming. Subsequently, there is a projected decrease in magnitude of the Guinea Coast rainfall extreme responses to this mode of climate variability in the three future periods, relative to the present-day situation. For the majority of the indices, the average of the changes in the teleconnection amplitude between the Guinea Coast and the eastern equatorial Atlantic indicates an enhancement in magnitude with time, and this increase becomes more robust for the long-term changes. However, although there is an overall increase in the total variance of most of the extreme indices over the Guinea Coast, there is a reduction in the contribution of the AEM to explain the variance of these extreme indices. This result suggests a weaker role of the AEM in driving the extreme rainfall variability over the Guinea Coast in a future scenario of high emission of greenhouse gases. Therefore, there is a need to identify other oceanic and atmospheric modes of variability or other processes that explain more the future changes in the extremes variability over the Guinea Coast. These processes should compensate for the decreasing role of the AEM. For instance, Akinsanola et al. (2020) argued that the changes in the circulation (the dynamics) should contribute less to the increase in the rainfall variability over West Africa, while the local thermodynamics should be the dominant factor of these changes.

Our conclusions are based on 24 CMIP6 GCMs that have clear biases and whose resolution is too coarse to represent well some important processes controlling extremes and their changes. It would thus be useful to reevaluate our results with RCMS

or even convection permitted models. The processes that drive the biases in the mean state and teleconnection patterns need also to be better understood and well represented, in order to gain more reliability on the projected changes in the rainfall extremes over the Guinea Coast.

505 **Appendix A: Additional figures**
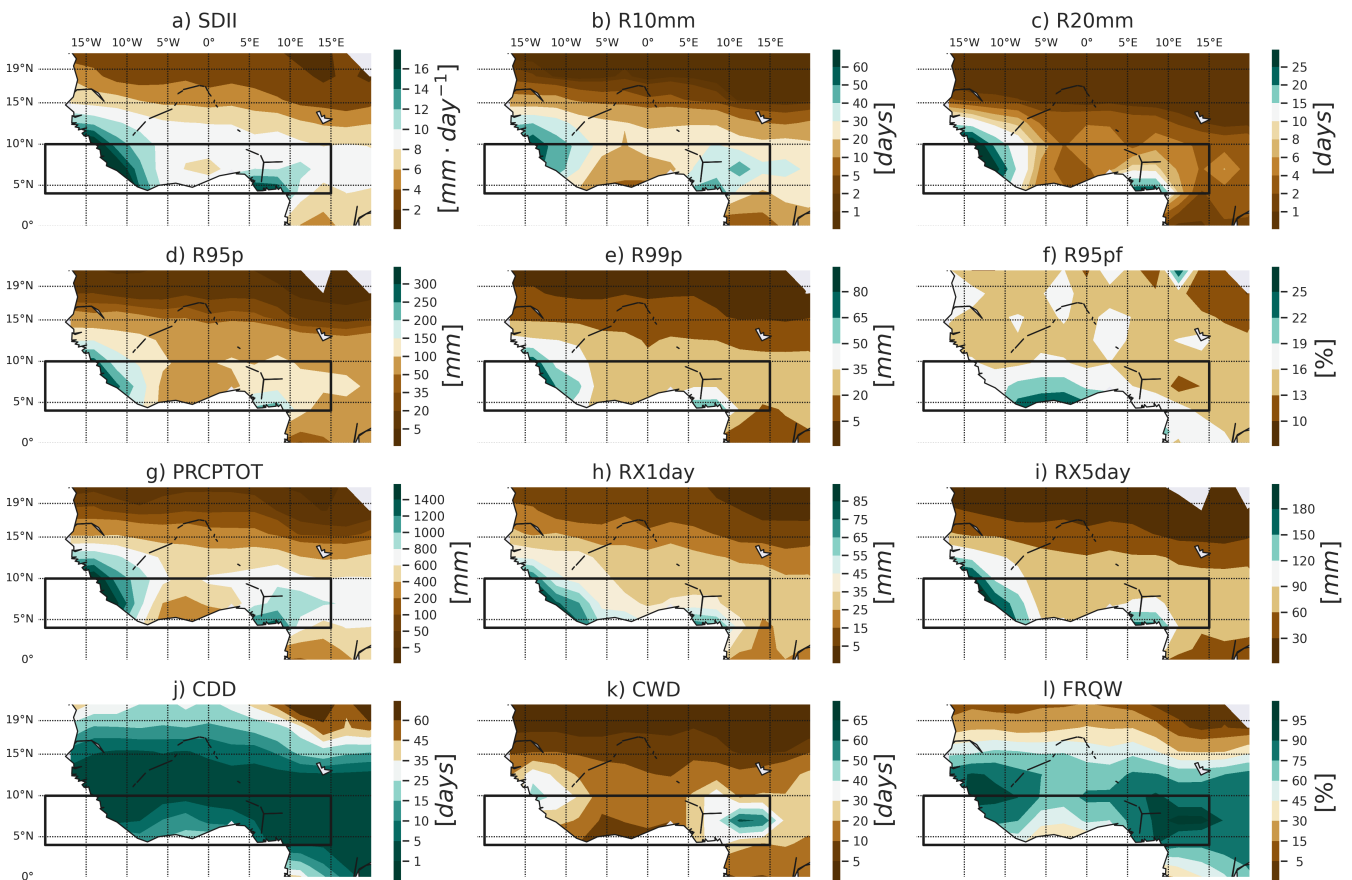
Figure A1. Spatial distribution of the mean JAS extreme rainfall indices over the 1995-2014 period from CHIRPS dataset. The black rectangles indicate the Guinea Coast region.
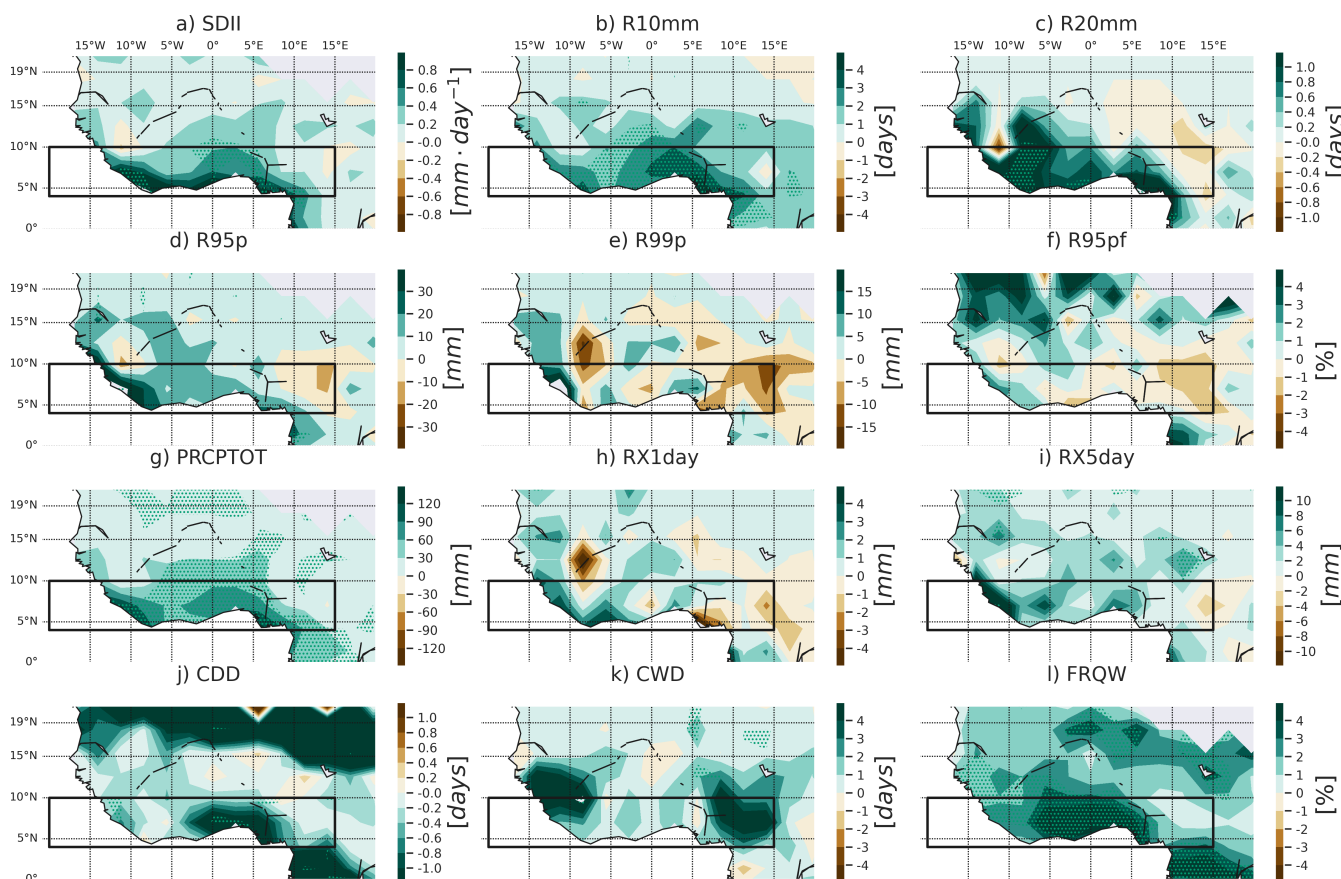
Figure A2. Maps of the JAS rainfall extreme indices (from CHIRPS dataset) regressed onto the standardized JAS AEM SST index (from HADISST dataset) over the 1995-2014 period. The stippling represents significant regression coefficient at 5% level according to a t-test. The black rectangles indicate the Guinea Coast region.

Author contributions. KW, TF and HG conceptualized the paper. KW performed the analyses, prepared the figures and wrote the manuscript based on the comments and suggestions from TF and HG.

Competing interests. The contact author has declared that neither they nor their co-authors have any competing interests

Acknowledgements. We acknowledge the World Climate Research Programme, which, through its Working Group on Coupled Modelling, coordinated and promoted CMIP6. We thank the climate modelling groups for producing and making available their model output, the Earth

510

System Grid Federation (ESGF) for archiving the data and providing access, and the multiple funding agencies who support CMIP6 and ESGF. Computational resources have been provided by the supercomputing facilities of the Université catholique de Louvain (CISM/U-CLouvain) and the Consortium des Equipements de Calcul Intensif en Fédération Wallonie Bruxelles (CECI) funded by the F.R.S.-FNRS under convention 2.5020.11. HG is research director with the Fonds de la Recherche Scientifique – FNRS (F.R.S.-FNRS).

515 **References**

Akinsanola, A. A. and Zhou, W.: Projections of West African summer monsoon rainfall extremes from two CORDEX models, Climate Dynamics, 52, 2017–2028, https://doi.org/10.1007/s00382-018-4238-8, 2019.

Akinsanola, A. A., Zhou, W., Zhou, T., and Keenlyside, N.: Amplification of synoptic to annual variability of West African summer monsoon rainfall under global warming, npj Climate and Atmospheric Science, 3, https://doi.org/10.1038/s41612-020-0125-1, 2020.

520 Akinsanola, A. A., Ongoma, V., and Kooperman, G. J.: Evaluation of CMIP6 models in simulating the statistics of extreme precipitation over Eastern Africa, Atmospheric Research, 254, 105 509, https://doi.org/10.1016/j.atmosres.2021.105509, 2021.

Atiah, W. A., Tsidu, G. M., Amekudzi, L. K., and Yorke, C.: Trends and interannual variability of extreme rainfall indices over Ghana, West Africa, Theoretical and Applied Climatology, 140, 1393–1407, https://doi.org/10.1007/s00704-020-03114-6, 2020.

Baidu, M., Schwendike, J., Marsham, J. H., and Bain, C.: Effects of vertical wind shear on intensities of mesoscale convective systems over
525 West and Central Africa, Atmospheric Science Letters, 23, e1094, https://doi.org/https://doi.org/10.1002/asl.1094, 2022.

Beucher, F., Lafore, J.-P., and Chapelon, N.: Simulation and analysis of the moist vortex associated with the extreme rain event of Ouagadougou in 2009, Quarterly Journal of the Royal Meteorological Society, 146, 86–104, https://doi.org/10.1002/qj.3645, 2019.

Bichet, A. and Diedhiou, A.: Less frequent and more intense rainfall along the coast of the Gulf of Guinea in West and Central Africa (1981-2014), Climate Research, 76, 191–201, https://doi.org/10.3354/cr01537, 2018.

530 Bjerknes, J.: Atmospheric teleconnections from the equatorial Pacific, Monthly Weather Review, 97, 163–172, https://doi.org/10.1175/1520-0493(1969)097<0163:atftep>2.3.co;2, 1969.

Crespo, L. R., Prigent, A., Keenlyside, N., Koseki, S., Svendsen, L., Richter, I., and Sánchez-Gómez, E.: Weakening of the Atlantic Niño variability under global warming, Nature Climate Change, https://doi.org/10.1038/s41558-022-01453-y, 2022.

Delhaye, S., Fichefet, T., Massonnet, F., Docquier, D., Msadek, R., Chripko, S., Roberts, C., Keeley, S., and Senan, R.: Summertime
535 changes in climate extremes over the peripheral Arctic regions after a sudden sea ice retreat, Weather and Climate Dynamics, 3, 555–573, https://doi.org/10.5194/wcd-3-555-2022, 2022.

Diatta, S. and Fink, A. H.: Statistical relationship between remote climate indices and West African monsoon variability, International Journal of Climatology, 34, 3348–3367, https://doi.org/10.1002/joc.3912, 2014.

Diatta, S., Diedhiou, C. W., Dione, D. M., and Sambou, S.: Spatial Variation and Trend of Extreme Precipitation in West Africa and Tele-
540 connections with Remote Indices, Atmosphere, 11, 999, https://doi.org/10.3390/atmos11090999, 2020.

Diedhiou, A., Bichet, A., Wartenburger, R., Seneviratne, S. I., Rowell, D. P., Sylla, M. B., Diallo, I., Todzo, S., Touré, N. E., Camara, M., Ngatchah, B. N., Kane, N. A., Tall, L., and Affholder, F.: Changes in climate extremes over West and Central Africa at 1.5 °C and 2 °C global warming, Environmental Research Letters, 13, 065 020, https://doi.org/10.1088/1748-9326/aac3e5, 2018.

Dike, V. N., Lin, Z.-H., and Ibe, C. C.: Intensification of Summer Rainfall Extremes over Nigeria during Recent Decades, Atmosphere, 11,
545 1084, https://doi.org/10.3390/atmos11101084, 2020.

Dosio, A., Jury, M. W., Almazroui, M., Ashfaq, M., Diallo, I., Engelbrecht, F. A., Klutse, N. A. B., Lennard, C., Pinto, I., Sylla, M. B., and Tamoffo, A. T.: Projected future daily characteristics of African precipitation based on global (CMIP5, CMIP6) and regional (CORDEX, CORDEX-CORE) climate models, Climate Dynamics, 57, 3135–3158, https://doi.org/10.1007/s00382-021-05859-w, 2021.

Elagib, N. A., Zayed, I. S. A., Saad, S. A., Mahmood, M. I., Basheer, M., and Fink, A. H.: Debilitating floods in the Sahel are becoming
550 frequent, Journal of Hydrology, 599, 126 362, https://doi.org/10.1016/j.jhydrol.2021.126362, 2021.

Engel, T., Fink, A. H., Knippertz, P., Pante, G., and Bliefernicht, J.: Extreme Precipitation in the West African Cities of Dakar and Ouagadougou: Atmospheric Dynamics and Implications for Flood Risk Assessments, Journal of Hydrometeorology, 18, 2937–2957, https://doi.org/10.1175/jhm-d-16-0218.1, 2017.

555 Eyring, V., Bony, S., Meehl, G. A., Senior, C. A., Stevens, B., Stouffer, R. J., and Taylor, K. E.: Overview of the Coupled Model Intercomparison Project Phase 6 (CMIP6) experimental design and organization, Geoscientific Model Development, 9, 1937–1958, https://doi.org/10.5194/gmd-9-1937-2016, 2016.

Faye, A. and Akinsanola, A. A.: Evaluation of extreme precipitation indices over West Africa in CMIP6 models, Climate Dynamics, https://doi.org/10.1007/s00382-021-05942-2, 2021.

Fofana, M., Adounkpe, J., Larbi, I., Hounkpe, J., Koubodana, H. D., Toure, A., Bokar, H., Dotse, S.-Q., and Limantol, 560 A. M.: Urban flash flood and extreme rainfall events trend analysis in Bamako, Mali, Environmental Challenges, 6, 100 449, https://doi.org/10.1016/j.envc.2022.100449, 2022.

Funk, C., Peterson, P., Landsfeld, M., Pedreros, D., Verdin, J., Shukla, S., Husak, G., Rowland, J., Harrison, L., Hoell, A., and Michaelsen, J.: The climate hazards infrared precipitation with stations–a new environmental record for monitoring extremes, Scientific Data, 2, 150 066, https://doi.org/10.1038/sdata.2015.66, 2015.

565 Gu, G. and Adler, R. F.: Seasonal Evolution and Variability Associated with the West African Monsoon System, Journal of Climate, 17, 3364–3377, https://doi.org/10.1175/1520-0442(2004)017<3364:seavaw>2.0.co;2, 2004.

Hegerl, G. C., Black, E., Allan, R. P., Ingram, W. J., Polson, D., Trenberth, K. E., Chadwick, R. S., Arkin, P. A., Sarojini, B. B., Becker, A., Dai, A., Durack, P. J., Easterling, D., Fowler, H. J., Kendon, E. J., Huffman, G. J., Liu, C., Marsh, R., New, M., Osborn, T. J., Skliris, N., Stott, P. A., Vidale, P.-L., Wijffels, S. E., Wilcox, L. J., Willett, K. M., and Zhang, X.: Challenges in Quantifying Changes in the Global 570 Water Cycle, Bulletin of the American Meteorological Society, 96, 1097 – 1115, https://doi.org/10.1175/BAMS-D-13-00212.1, 2015.

Jia, F., Cai, W., Wu, L., Gan, B., Wang, G., Kucharski, F., Chang, P., and Keenlyside, N.: Weakening Atlantic Niño–Pacific connection under greenhouse warming, Science Advances, 5, eaax4111, https://doi.org/10.1126/sciadv.aax4111, 2019.

Klutse, N. A. B., Ajayi, V. O., Gbobaniyi, E. O., Egbebiyi, T. S., Kouadio, K., Nkrumah, F., Quagraine, K. A., Olusegun, C., Diasso, U., Abiodun, B. J., Lawal, K., Nikulin, G., Lennard, C., and Dosio, A.: Potential impact of 1.5 °C and 2 °C global warming on consecutive 575 dry and wet days over West Africa, Environmental Research Letters, 13, 055 013, https://doi.org/10.1088/1748-9326/aab37b, 2018.

Klutse, N. A. B., Quagraine, K. A., Nkrumah, F., Quagraine, K. T., Berkoh-Oforiwaa, R., Dzrobi, J. F., and Sylla, M. B.: The Climatic Analysis of Summer Monsoon Extreme Precipitation Events over West Africa in CMIP6 Simulations, Earth Systems and Environment, 5, 25–41, https://doi.org/10.1007/s41748-021-00203-y, 2021.

Kpanou, M., Laux, P., Brou, T., Vissin, E., Camberlin, P., and Roucou, P.: Spatial patterns and trends of extreme rainfall over the southern 580 coastal belt of West Africa, Theoretical and Applied Climatology, 143, 473–487, https://doi.org/10.1007/s00704-020-03441-8, 2020.

Lafore, J.-P., Beucher, F., Peyrillé, P., Diongue-Niang, A., Chapelon, N., Bouniol, D., Caniaux, G., Favot, F., Ferry, F., Guichard, F., Poan, E., Roehrig, R., and Vischel, T.: A multi-scale analysis of the extreme rain event of Ouagadougou in 2009, Quarterly Journal of the Royal Meteorological Society, 143, 3094–3109, https://doi.org/10.1002/qj.3165, 2017.

Li, C., Zwiers, F., Zhang, X., Li, G., Sun, Y., and Wehner, M.: Changes in Annual Extremes of Daily Temperature and Precipitation in CMIP6 585 Models, Journal of Climate, 34, 3441–3460, https://doi.org/10.1175/jcli-d-19-1013.1, 2021a.

Li, T., Jiang, Z., Treut, H. L., Li, L., Zhao, L., and Ge, L.: Machine learning to optimize climate projection over China with multi-model ensemble simulations, Environmental Research Letters, 16, 094 028, https://doi.org/10.1088/1748-9326/ac1d0c, 2021b.

Losada, T., Rodriguez-Fonseca, B., Mohino, E., Bader, J., Janicot, S., and Mechoso, C. R.: Tropical SST and Sahel rainfall: A non-stationary relationship, Geophys. Res. Lett., 39, https://doi.org/10.1029/2012GL052423, 2012.

590 Lübbecke, J. F., Rodríguez-Fonseca, B., Richter, I., Martín-Rey, M., Losada, T., Polo, I., and Keenlyside, N. S.: Equatorial Atlantic variability-Modes, mechanisms, and global teleconnections, Wiley Interdisciplinary Reviews: Climate Change, 9, e527, https://doi.org/10.1002/wcc.527, 2018.

Maranan, M., Fink, A. H., Knippertz, P., Francis, S. D., Akpo, A. B., Jegede, G., and Yorke, C.: Interactions between Convection and a Moist Vortex Associated with an Extreme Rainfall Event over Southern West Africa, Monthly Weather Review, 147, 2309–2328,
595 https://doi.org/10.1175/mwr-d-18-0396.1, 2019.

Mearns, L., Giorgi, F., McDaniel, L., and Shields, C.: Analysis of daily variability of precipitation in a nested regional climate model: comparison with observations and doubled CO2 results, Global and Planetary Change, 10, 55–78, https://doi.org/https://doi.org/10.1016/0921-8181(94)00020-E, results from the Model Evaluation Consortium for Climate Assessment, 1995.

Mouhamed, L., Traore, S. B., Alhassane, A., and Sarr, B.: Evolution of some observed climate extremes in the West African Sahel, Weather
600 and Climate Extremes, 1, 19–25, https://doi.org/10.1016/j.wace.2013.07.005, 2013.

New, M., Hewitson, B., Stephenson, D. B., Tsiga, A., Kruger, A., Manhique, A., Gomez, B., Coelho, C. A. S., Masisi, D. N., Kululanga, E., Mbambalala, E., Adesina, F., Saleh, H., Kanyanga, J., Adosi, J., Bulane, L., Fortunata, L., Mdoka, M. L., and Lajoie, R.: Evidence of trends in daily climate extremes over southern and west Africa, Journal of Geophysical Research, 111, https://doi.org/10.1029/2005jd006289, 2006.

605 Odoulami, R. C. and Akinsanola, A. A.: Recent assessment of West African summer monsoon daily rainfall trends, Weather, 73, 283–287, https://doi.org/10.1002/wea.2965, 2017.

O'Neill, B. C., Tebaldi, C., van Vuuren, D. P., Eyring, V., Friedlingstein, P., Hurtt, G., Knutti, R., Kriegler, E., Lamarque, J.-F., Lowe, J., Meehl, G. A., Moss, R., Riahi, K., and Sanderson, B. M.: The Scenario Model Intercomparison Project (ScenarioMIP) for CMIP6, Geoscientific Model Development, 9, 3461–3482, https://doi.org/10.5194/gmd-9-3461-2016, 2016.

610 Polo, I., Rodríguez-Fonseca, B., Losada, T., and García-Serrano, J.: Tropical Atlantic Variability Modes (1979–2002). Part I: Time-Evolving SST Modes Related to West African Rainfall, Journal of Climate, 21, 6457–6475, https://doi.org/10.1175/2008JCLI2607.1, 2008.

Rayner, N. A., Parker, D. E., Horton, E. B., Folland, C. K., Alexander, L. V., Rowell, D. P., Kent, E. C., and Kaplan, A.: Global analyses of sea surface temperature, sea ice, and night marine air temperature since the late nineteenth century, Journal of Geophysical Research: Atmospheres, 108, https://doi.org/https://doi.org/10.1029/2002JD002670, 2003.

615 Rehfeld, K., Hébert, R., Lora, J. M., Lofverstrom, M., and Brierley, C. M.: Variability of surface climate in simulations of past and future, Earth System Dynamics, 11, 447–468, https://doi.org/10.5194/esd-11-447-2020, 2020.

Richter, I. and Tokinaga, H.: An overview of the performance of CMIP6 models in the tropical Atlantic: mean state, variability, and remote impacts, Climate Dynamics, 55, 2579–2601, https://doi.org/10.1007/s00382-020-05409-w, 2020.

Rind, D., Goldberg, R., and Ruedy, R.: Change in climate variability in the 21st century, Climatic Change, 14, 5–37,
620 https://doi.org/10.1007/BF00140173, 1989.

Rodríguez-Fonseca, B., Mohino, E., Mechoso, C. R., Caminade, C., Biasutti, M., Gaetani, M., Garcia-Serrano, J., Vizy, E. K., Cook, K., Xue, Y., Polo, I., Losada, T., Druyan, L., Fontaine, B., Bader, J., Doblas-Reyes, F. J., Goddard, L., Janicot, S., Arribas, A., Lau, W., Colman, A., Vellinga, M., Rowell, D. P., Kucharski, F., and Voldoire, A.: Variability and Predictability of West African Droughts: A Review on the Role of Sea Surface Temperature Anomalies, Journal of Climate, 28, 4034–4060, https://doi.org/10.1175/JCLI-D-14-00130.1, 2015.

625 Sanogo, S., Peyrillé, P., Roehrig, R., Guichard, F., and Ouedraogo, O.: Extreme Precipitating Events in Satellite and Rain Gauge Products over the Sahel, Journal of Climate, 35, 1915–1938, https://doi.org/10.1175/jcli-d-21-0390.1, 2022.

Schubert, S. D., Stewart, R. E., Wang, H., Barlow, M., Berbery, E. H., Cai, W., Hoerling, M. P., Kanikicharla, K. K., Koster, R. D., Lyon, B., Mariotti, A., Mechoso, C. R., Müller, O. V., Rodriguez-Fonseca, B., Seager, R., Seneviratne, S. I., Zhang, L., and Zhou, T.: Global Meteorological Drought: A Synthesis of Current Understanding with a Focus on SST Drivers of Precipitation Deficits, Journal of Climate,

630 29, 3989–4019, https://doi.org/10.1175/JCLI-D-15-0452.1, 2016.

Seneviratne, S. I., Zhang, X., Adnan, M., Badi, W., Dereczynski, C., Luca, A. D., Ghosh, S., Iskandar, I., Kossin, J., Lewis, S., Otto, F., Pinto, I., Satoh, M., Vicente-Serrano, S. M., Wehner, M., and Zhou, B.: Climate Change 2021: The Physical Science Basis. Contribution of Working Group I to the Sixth Assessment Report of the Intergovernmental Panel on Climate Change, chap. Weather and climate extreme events in a changing climate, Cambridge University Press. In Press., 2021.

635 Sillmann, J., Kharin, V. V., Zhang, X., Zwiers, F. W., and Bronaugh, D.: Climate extremes indices in the CMIP5 multimodel ensemble: Part 1. Model evaluation in the present climate, Journal of Geophysical Research: Atmospheres, 118, 1716–1733, https://doi.org/10.1002/jgrd.50203, 2013a.

Sillmann, J., Kharin, V. V., Zwiers, F. W., Zhang, X., and Bronaugh, D.: Climate extremes indices in the CMIP5 multimodel ensemble: Part 2. Future climate projections, Journal of Geophysical Research: Atmospheres, 118, 2473–2493, https://doi.org/10.1002/jgrd.50188, 2013b.

640 Survey, U. S. G., Funk, C. C., Peterson, P. J., Landsfeld, M. F., Pedreros, D. H., Verdin, J. P., Rowland, J. D., Romero, B. E., Husak, G. J., Michaelsen, J. C., and Verdin, A. P.: A quasi-global precipitation time series for drought monitoring, Tech. rep., Reston, VA, https://doi.org/10.3133/ds832, 2014.

Taylor, K. E.: Summarizing multiple aspects of model performance in a single diagram, Journal of Geophysical Research: Atmospheres, 106, 7183–7192, https://doi.org/10.1029/2000jd900719, 2001.

645 Thiery, W., Lange, S., Rogelj, J., Schleussner, C.-F., Gudmundsson, L., Seneviratne, S. I., Andrijevic, M., Frieler, K., Emanuel, K., Geiger, T., Bresch, D. N., Zhao, F., Willner, S. N., Büchner, M., Volkholz, J., Bauer, N., Chang, J., Ciais, P., Dury, M., François, L., Grillakis, M., Gosling, S. N., Hanasaki, N., Hickler, T., Huber, V., Ito, A., Jägermeyr, J., Khabarov, N., Koutroulis, A., Liu, W., Lutz, W., Mengel, M., Müller, C., Ostberg, S., Reyer, C. P. O., Stacke, T., and Wada, Y.: Intergenerational inequities in exposure to climate extremes, Science, 374, 158–160, https://doi.org/10.1126/science.abi7339, 2021.

650 Thorncroft, C. D. and Hoskins, B. J.: An idealized study of African easterly waves. I: A linear view, Quarterly Journal of the Royal Meteorological Society, 120, 953–982, https://doi.org/10.1002/qj.49712051809, 1994a.

Thorncroft, C. D. and Hoskins, B. J.: An idealized study of African easterly waves. II: A nonlinear view, Quarterly Journal of the Royal Meteorological Society, 120, 983–1015, https://doi.org/10.1002/qj.49712051810, 1994b.

Tokinaga, H. and Xie, S.-P.: Weakening of the equatorial Atlantic cold tongue over the past six decades, Nature Geoscience, 4, 222–226,

655 https://doi.org/10.1038/ngeo1078, 2011.

United Nations Office for the Coordination of Humanitarian Affairs (OCHA): Note de Synthèse : Impact des inondations Afrique de l'Ouest et du Centre, United Nations, https://reliefweb.int/sites/reliefweb.int/files/resources/SynthèsesurlesinondationsAfriquedelOuestetduCentre. pdf, 2012.

United Nations Office for the Coordination of Humanitarian Affairs (OCHA): ANNUAL REPORT 2020, United Nations, https://www.

660 unocha.org/sites/unocha/files/2020%20OCHA%20annual%20report.pdf, 2021.

van der Wiel, K. and Bintanja, R.: Contribution of climatic changes in mean and variability to monthly temperature and precipitation extremes, Communications Earth & Environment, 2, https://doi.org/10.1038/s43247-020-00077-4, 2021.

Wainwright, C. M., Black, E., and Allan, R. P.: Future Changes in Wet and Dry Season Characteristics in CMIP5 and CMIP6 Simulations, Journal of Hydrometeorology, 22, 2339 – 2357, https://doi.org/10.1175/JHM-D-21-0017.1, 2021.

665 Worou, K., Goosse, H., Fichefet, T., Guichard, F., and Diakhate, M.: Interannual variability of rainfall in the Guinean Coast region and its links with sea surface temperature changes over the twentieth century for the different seasons, Climate Dynamics, 55, 449–470, https://doi.org/10.1007/s00382-020-05276-5, 2020.

Worou, K., Goosse, H., Fichefet, T., and Kucharski, F.: Weakened impact of the Atlantic Niño on the future equatorial Atlantic and Guinea Coast rainfall, Earth System Dynamics, 13, 231–249, https://doi.org/10.5194/esd-13-231-2022, 2022.

670 Yang, Y., Wu, L., Cai, W., Jia, F., Ng, B., Wang, G., and Geng, T.: Suppressed Atlantic Niño/Niña variability under greenhouse warming, Nature Climate Change, https://doi.org/10.1038/s41558-022-01444-z, 2022.

Zebiak, S. E.: Air–Sea Interaction in the Equatorial Atlantic Region, Journal of Climate, 6, 1567 – 1586, https://doi.org/10.1175/1520-0442(1993)006<1567:AIITEA>2.0.CO;2, 1993.